Nucleic Acids Research, 2018 **1**
doi: 10.1093/nar/gky478

Transfer-matrix calculations of the effects of tension and torque constraints on DNA–protein interactions

Artem K. Efremov[1,2,*] and Jie Yan[1,2,3,*]

[1]Mechanobiology Institute, National University of Singapore, 117411, Singapore, [2]Centre for Bioimaging Sciences, National University of Singapore, 117557, Singapore and [3]Department of Physics, National University of Singapore, 117551, Singapore

Received February 10, 2018; Revised May 09, 2018; Editorial Decision May 15, 2018; Accepted May 17, 2018

ABSTRACT

Organization and maintenance of the chromosomal DNA in living cells strongly depends on the DNA interactions with a plethora of DNA-binding proteins. Single-molecule studies show that formation of nucleoprotein complexes on DNA by such proteins is frequently subject to force and torque constraints applied to the DNA. Although the existing experimental techniques allow to exert these type of mechanical constraints on individual DNA biopolymers, their exact effects in regulation of DNA–protein interactions are still not completely understood due to the lack of systematic theoretical methods able to efficiently interpret complex experimental observations. To fill this gap, we have developed a general theoretical framework based on the transfer-matrix calculations that can be used to accurately describe behaviour of DNA–protein interactions under force and torque constraints. Potential applications of the constructed theoretical approach are demonstrated by predicting how these constraints affect the DNA-binding properties of different types of architectural proteins. Obtained results provide important insights into potential physiological functions of mechanical forces in the chromosomal DNA organization by architectural proteins as well as into single-DNA manipulation studies of DNA–protein interactions.

INTRODUCTION

DNA-architectural proteins play a major role in the genome structural organization and maintenance of its functionality in living cells, regulating a delicate balance between the chromosomal DNA condensation level and its accessibility to various DNA-binding proteins. By synergistically cooperating or antagonizing each other's action on the chromosomal DNA, architectural proteins can adjust its mechanical properties, compaction level and supercoiling state on a local as well as the global genome scales, affecting the transcription level of numerous genes in living cells. Thus, by regulating the DNA-binding properties of architectural proteins, cells can dynamically change organization of the chromosomal DNA and rapidly switch between different gene expression patterns in response to environmental cues (1–3).

While DNA-architectural proteins are the key components determining the chromosomal DNA organization, it should be noted that they perform their function in the context of numerous mechanical constraints imposed on the DNA by various factors, such as multiple DNA motor proteins [topoisomerases, helicases, RNA/DNA polymerases, etc. (4–9)], that generate stretching and twisting forces on the chromosomal DNA (10–15). It is also known that chromosomes form extensive adhesion contacts with a number of nuclear membrane proteins, establishing force-transmitting links between the chromosomal DNA and cytoplasmic cytoskeleton, which frequently carries strong mechanical loads (16–18). As a result, the chromosomal DNA is a subject to the combined action of both DNA-architectural proteins and the mechanical constraints applied to it. Together, these factors not only determine the physical organization of the chromosomal DNA, but also play the major role in gene transcription regulation inside living cells.

Indeed, it has been revealed in recent experiments that cells not only use various mechanical constraints to shape the chromosomal DNA, but actually can sense and process mechanical forces applied to the nucleus, changing the level of genes' transcription in response to their action (17–21). While the exact molecular processes responsible for such mechanosensing of living cells remain unclear, recent experimental studies suggest that this may be the result of force- and torque-dependent interactions between different groups of DNA-architectural proteins and chromosomal DNA.

*To whom correspondence should be addressed. Tel: +65 65162620; Fax: +65 67776126; Emails: mbiay@nus.edu.sg (A.K.E.) and phyyj@nus.edu.sg (J.Y.)

Namely, crystallographic and single-molecule experiments show that upon binding to DNA proteins frequently prompt various conformational changes in the DNA structure, which can be coupled to force and torque constraints applied to the DNA, affecting the DNA-binding properties of proteins (22–34). What is even more interesting, existing experimental data indicate that different groups of DNA-architectural proteins frequently produce very distinct responses to the applied mechanical constraints. Indeed, according to their mechanism of interaction with DNA all architectural proteins can be divided into four major groups (1): (i) DNA-wrapping proteins, which fold DNA into compact nucleoprotein complexes (such as eukaryotic/archaeal histones) (23,24,35); (ii) DNA-bending proteins, which sharply curve DNA at the protein binding site (like bacterial HU, IHF and Fis) (22,25–28,30,32,36); (iii) DNA-bridging proteins that cross-link DNA duplexes (e.g. bacterial H-NS, human HMGA2 or any other protein that mediates DNA loops) (29,37–39) and (iv) DNA-stiffening proteins forming rigid nucleoprotein filaments along DNA (like archaeal TrmBL2 and Alba) (31,33,40). Thus, the four major groups of DNA-architectural proteins form nucleoprotein complexes, which have very different 3D structures, leading to diverse responses of these proteins to force and torque constraints applied to DNA.

For example, previous studies have shown that while suppressing formation of nucleoprotein complexes by DNA-bending and DNA-wrapping proteins, mechanical stretching of DNA promotes its interaction with DNA-stiffening proteins (32,36,41–44). Likewise, torque exerted on DNA can either enhance or weaken binding of DNA-wrapping proteins depending on the chirality of the resulting nucleoprotein complexes and the direction of the applied torque (45). Such a differential response of proteins to mechanical constraints applied to DNA suggests that it is possible to shift balance between nucleoprotein complexes formed by different groups of proteins in favour of one or the other protein group by changing the applied constraints (33).

Indeed, as experimental data show, this mechanism is frequently used by living cells to organize their chromosomal DNA. For example, topoisomerases I and II relax positive (right-handed) torsion accumulated in DNA during chromosome condensation by architectural proteins (histones) or due to DNA replication/transcription processes, allowing continuous assembly of left-handed nucleosome complexes that would not otherwise form on positively supercoiled DNA (46–48). This type of DNA organization control even more pronounced in bacterial cells, which use gyrases to maintain negatively supercoiled state of their circular chromosomal DNA to promote its interaction on a local and the global scales with various DNA-architectural proteins, such as H-NS and HU (49–51).

To better understand potential roles of mechanical constraints in regulation of DNA interactions with architectural proteins, a number of single-DNA manipulation experimental methods have been recently developed, allowing one to control the supercoiling state of individual DNA molecules as well as to apply force and torque constraints to them (52–61). While such experiments may provide important information regarding the effects of mechanical constraints onto the DNA-binding properties of architectural proteins, it should be noted that typical observables measured in these experiments, such as the DNA extension and linking number change, frequently have highly complex dependence on the force and torque constraints applied to the DNA, especially in the presence of DNA-binding proteins in solution. As a result, interpretation of the collected experimental data poses a challenging task that requires development of a general theoretical framework aimed at description of DNA-binding behaviour of architectural proteins in a wide range of force and torque constraints applied to DNA.

So far, most of the previous theoretical studies have been mainly focussed on understanding of the effects of stretching force on protein binding to a torsionally relaxed DNA, proposing several different approaches to investigate this question (42,44,62–73). Among the proposed methods, the transfer-matrix theory developed based on a discretized semi-flexible polymer chain model of DNA has several unique advantages by providing very fast semi-analytical calculations of equilibrium conformations of DNA that allow one to easily incorporate DNA heterogeneity into the computations (42,64,69,74).

Furthermore, by using several famous results from the group theory, it has been recently shown that the transfer-matrix formalism can be further extended to take into consideration not only force, but also torque constraints, considerably increasing the scope of its potential applications, including but not limited to description of local DNA structural transitions and sequence-dependent response of DNA to stretching and torsional strains (75,76). What is even more important, this advancement in the transfer-matrix calculations opens a completely new way to development of a general theoretical framework aimed at description of DNA–protein interactions under both force and torque constraints.

In this study, we show in details how such theoretical framework can be constructed based on the mathematical formalism described in ref. (75,76) and demonstrate how the developed theoretical approach can be used to obtain insights into potential roles of force and torque constraints in regulation of DNA interaction with different types of DNA-binding proteins found in living cells.

MATERIALS AND METHODS

Theoretical calculations

All the computations presented in this study were done by using in-house written software developed in Matlab 8.5.0. The source code of the simplified versions of the programs can be downloaded from the personal websites of the authors: www.artem-efremov.org (A.K.E.) and www.physics.nus.edu.sg/~biosmm/ (J.Y.).

Experimental data

The force-extension curves of DNA in the presence of TrmBL2 protein in solution were measured by using transverse magnetic tweezers. The details of the protein expression, purification and single-DNA stretching experiments can be found in our previous publication (33).

GENERAL THEORY

Brief outline of the theoretical framework

In our previous work, it has been shown that DNA behaviour under mechanical constraints can be accurately described by a semiflexible polymer model in which DNA is represented by a polygonal chain consisting of straight segments whose 3D orientations in space are characterized by the three Euler rotation angles, see Figure 1A and B. Introducing transfer-matrices defined on each of the vertices joining neighbouring DNA segments, it is then possible to calculate the DNA partition function and obtain detailed information regarding the DNA conformation and DNA structural fluctuations under force and torque constraints (75,76). In this study, we describe how the previously developed transfer-matrix formalism can be further expanded to integrate DNA–protein interactions into the model. While all of the details can be found in Supplementary Appendices A–G, in this section we will mainly focus on the central ideas and assumptions underlying the transfer-matrix calculations for DNA behaviour under force and torque constraints in the presence of DNA–protein interactions.

As before, DNA will be represented by a discretized polygonal chain consisting of short segments, which are treated as rigid bodies with a local coordinate system $(\mathbf{x}_j, \mathbf{y}_j, \mathbf{z}_j)$ attached to each of the DNA segments, see schematic Figure 1A. Here j is the index enumerating all of the DNA segments from 1 to N, where N is the total number of segments in the discretized polymer chain representing DNA molecule. 3D orientation of each of the coordinate systems, and thus each of the DNA segments, is then can be described by the Euler rotation matrix $\mathbf{R}_j = \mathbf{R}_{\alpha_j}\mathbf{R}_{\beta_j}\mathbf{R}_{\gamma_j}$ resulting from the composition of three successive revolutions through Euler angles α_j, β_j and γ_j about the fixed lab coordinate frame $(\mathbf{x}_0, \mathbf{y}_0, \mathbf{z}_0)$, see Figure 1B.

Besides the 3D orientation, DNA segments in addition are characterized by their physical state. Namely, existing experimental data show that depending on the force and torque constraints applied to DNA it may exist in several different structural states known as B-, L-, P-DNA, etc. (56,77–82). For the sake of simplicity, in this study we consider only the following structural states of DNA, which are the most relevant to the physiological ranges of forces and torques: (i) B-DNA state, which is typical for relaxed DNA polymer; (ii) L-DNA, which is favoured at negative torques and (iii) P-DNA, which is favoured at positive torques, see more detailed description of these DNA forms in ref. (75,76). Thus, in the absence of protein binding, the DNA conformation is completely determined by the two sets of parameters: (i) rotation matrices $(\mathbf{R}_1, ..., \mathbf{R}_N)$ describing orientations of all DNA segments, and (ii) indexes $(k_1, ..., k_N)$ representing the structural states of these segments, such that for each segment $j = 1, ..., N$ we put $k_j = 0$ for B-DNA segments, $k_j = -1$—for L-DNA segments and $k_j = -2$—for P-DNA segments.

Incorporation of DNA–protein interactions into the model results in appearance of additional DNA segment states. Indeed, besides indexes $k_j = -2, -1$ and 0 ($j = 1, ..., N$) that indicate the structural states of bare DNA segments, we also need to have a mean to describe the states of DNA segments residing inside nucleoprotein complexes formed on DNA. Namely, to mark the positions of DNA segments in each of the nucleoprotein complexes, we will use positive values for indexes k_j that will designate the sequence number of each DNA segment with respect to the DNA entry point into the complex. In other words, assuming that the protein of interest occupies K DNA segments upon binding to DNA, one can assign K DNA binding sites on the protein surface—from 1 (the first DNA binding site on the protein surface) to K (the last DNA binding site on the protein surface). Correspondingly, for each DNA segment bound to the protein we put the value of k_j equal to the index of the respective binding site on the surface of the protein—from $k_j = 1$ (if the DNA segment is bound to the first binding site on the protein surface) to $k_j = K$ (if the DNA segment is bound to the last binding site on the protein surface). Thus, in the presence of DNA–protein interactions, indexes k_j ($j = 1, ..., N$) take integer values in the range from -2 to K, with $k_j = -2, -1, 0$ representing bare DNA segments being in P-, L- or B-DNA states, respectively; and $k_j = 1, ..., K$ corresponding to protein-bound DNA segments. In the latter case, for a given DNA segment, j, parameter k_j equals to the index of the DNA binding site on the protein surface to which this DNA segment is bound. As an example, see schematic figure Figure 1C for the case of $K = 12$.

In the general case, the total conformational energy of DNA interacting with proteins, E_{tot}, can be written as a sum of the following energy terms:

$$E_{\text{tot}}(k_1...k_N, \mathbf{R}_1...\mathbf{R}_N) = E_{\text{DNA}} + E_{\text{protein}} + \Phi_f + \Phi_\tau \quad (1)$$

Here E_{DNA} is the sum of the bending and twisting deformation energies of all protein-unbound bare DNA segments, and E_{protein} is the sum of the energies associated with nucleoprotein complexes formed on the DNA. Furthermore, $\Phi_f = -(\mathbf{f}\cdot\mathbf{d})$ is the potential energy related to the stretching force $\mathbf{f}$ applied to the DNA, where $\mathbf{d}$ denotes the DNA end-to-end vector; and $\Phi_\tau = -2\pi\tau\Delta\text{Lk}$ is the potential energy associated with the torque τ applied to the DNA, where ΔLk denotes the DNA linking number change with respect to the torsionally relaxed B-DNA state, which is used in this study as a reference state for the energy calculations. For the sake of simplicity, all of the energies in this study are presented in k_BT units, where k_B is Boltzmann constant and T is temperature of the surrounding environment. For this reason, the force $\mathbf{f}$ and torque τ are scaled by k_BT; thus, $\mathbf{f}$ has a dimension of 1/length and τ is dimensionless.

While the above energy terms will be discussed in details in the next section, here we only would like to stress that under very general assumptions it is possible to represent the total conformational energy of DNA, E_{tot}, as a sum of local DNA segment contributions [see Supplementary Appendix B]:

$$E_{\text{tot}}(k_1...k_N, \mathbf{R}_1...\mathbf{R}_N) = \sum_{j=1}^{N-1} E_{k_jk_{j+1}}(\mathbf{R}_j, \mathbf{R}_{j+1}) + E_{k_Nk_1}(\mathbf{R}_N, \mathbf{R}_1) \quad (2)$$

Where $E_{k_jk_{j+1}}(\mathbf{R}_j, \mathbf{R}_{j+1})$ is the local energy contribution by the jth vertex in the polygonal chain representing DNA that joins the jth and the $(j+1)$th DNA segments.

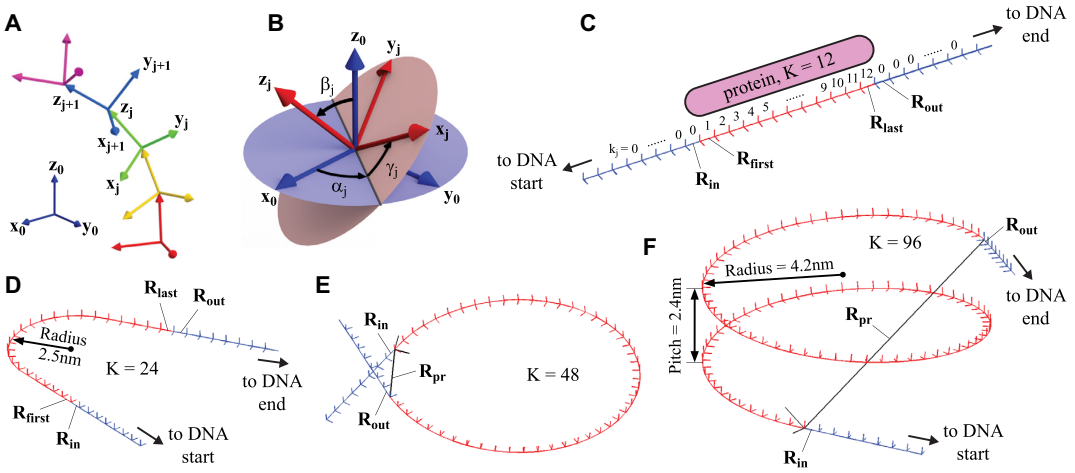

Figure 1. Semiflexible polymer chain model of DNA. (**A**) In the model, DNA is represented by a polygonal chain comprised of straight segments. The latter are considered as rigid bodies with attached local Cartesian coordinate frames, $(\mathbf{x}_j, \mathbf{y}_j, \mathbf{z}_j)$, whose 3D-orientations in space with respect to the fixed global coordinate system $(\mathbf{x}_0, \mathbf{y}_0, \mathbf{z}_0)$ are described by the Euler rotation matrices, $\mathbf{R}_j$. (**B**) Each rotation matrix, $\mathbf{R}_j$, results from the composition of three successive revolutions of the coordinate frame $(\mathbf{x}_j, \mathbf{y}_j, \mathbf{z}_j)$ relative to the fixed coordinate system $(\mathbf{x}_0, \mathbf{y}_0, \mathbf{z}_0)$ through Euler angles α_j, β_j and γ_j shown on the graph. (**C**–**F**) Proteins binding to DNA results in formation of nucleoprotein complexes that constrain protein-bound DNA segments in a specific 3D conformation: DNA-stiffening proteins typically form straight nucleoprotein filaments along DNA (C), while DNA-bending proteins kink DNA at the binding site (D); as for DNA-wrapping proteins, such as histone tetramers and octamers, their interaction with DNA results in formation of solenoid-like nucleoprotein complexes (E and F). On panels (C–F), bare DNA segments are shown in blue color and protein-bound DNA segments forming the respective nucleoprotein complexes are presented in red colour. On panel (C), indexes k_j, which are displayed above the DNA segments, indicate the physical states of the corresponding segments.

$E_{k_jk_{j+1}}(\mathbf{R}_j, \mathbf{R}_{j+1})$ in the general case depends on the states k_j and k_{j+1} of the jth and the $(j+1)$th DNA segments as well as their orientations, $\mathbf{R}_j$ and $\mathbf{R}_{j+1}$. The last term in Equation (2) describes the contribution of the DNA end segments, which may be considered as a part of boundary conditions imposed on the DNA.

Knowing the total conformational energy of DNA, it is then straightforward to find its partition function, $Z_{f,\tau}$, which can be calculated as:

$$Z_{f,\tau} = \sum_{k_1 \ldots k_N=-2}^{K} \int d\mathbf{R}_1 \ldots d\mathbf{R}_N \, d[\eta_{in}] \, \xi(\mathbf{R}_N, \mathbf{R}_1) \times e^{-E_{tot}(k_1 \ldots k_N, \mathbf{R}_1 \ldots \mathbf{R}_N)} \quad (3)$$

Where $\xi(\mathbf{R}_N, \mathbf{R}_1)$ is a function that imposes specific boundary conditions on the orientations of the DNA end segments. In the above formula, integrations are carried out over all of the DNA segment orientations, $(\mathbf{R}_1, ..., \mathbf{R}_N)$. Furthermore, in order to take into account orientational freedom of nucleoprotein complexes, we in addition perform integration $\int d[\eta_{in}]$ over all possible rotations of these complexes with respect to the axes of the DNA segments entering them, for more details see comments after Equation (B11) in Supplementary Appendix B.

Substituting Equation (2) into Equation (3), it can be shown that the exponent in Equation (3) can be re-written as a product of local transfer-functions, $T_{k_jk_{j+1}}(\mathbf{R}_j, \mathbf{R}_{j+1})$, defined on the vertices joining neighbouring DNA segments, where $T_{k_jk_{j+1}}(\mathbf{R}_j, \mathbf{R}_{j+1}) = \int d\eta_{in} \, e^{-E_{k_jk_{j+1}}(\mathbf{R}_j, \mathbf{R}_{j+1})}$ if the jth and $(j+1)$th DNA segments are located at the interface between bare DNA and one of the nulceoprotein complexes, such that $(k_j, k_{j+1}) = (0, 1)$, $(-1, 1)$ or $(-2, 1)$; and $T_{k_jk_{j+1}}(\mathbf{R}_j, \mathbf{R}_{j+1}) = e^{-E_{k_jk_{j+1}}(\mathbf{R}_j, \mathbf{R}_{j+1})}$ in all other cases [for more details see Supplementary Appendices C and G]. Indeed, from Equations (2), (3) and the above definition of local DNA transfer-functions, it is not hard to see that the partition function, $Z_{f,\tau}$, turns into:

$$Z_{f,\tau} = \sum_{k_1 \ldots k_N=-2}^{K} \int d\mathbf{R}_1 \ldots d\mathbf{R}_N \prod_{j=1}^{N-1} T_{k_jk_{j+1}}(\mathbf{R}_j, \mathbf{R}_{j+1}) \times \sigma_{k_Nk_1}(\mathbf{R}_N, \mathbf{R}_1) \quad (4)$$

Here all of the $\int d[\eta_{in}]$ integrals from Equation (3) are adsorbed into $T_{k_j1}(\mathbf{R}_j, \mathbf{R}_{j+1})$ transfer-functions corresponding to the DNA segments entering nucleoprotein complexes. As for $\sigma_{k_Nk_1}(\mathbf{R}_N, \mathbf{R}_1)$ functions, they describe the boundary conditions imposed on the DNA end segments and have the following simple form:

$$\sigma_{k_Nk_1}(\mathbf{R}_N, \mathbf{R}_1) = \xi(\mathbf{R}_N, \mathbf{R}_1) \, e^{-E_{k_Nk_1}(\mathbf{R}_N, \mathbf{R}_1)} \quad (5)$$

Where $E_{k_Nk_1}(\mathbf{R}_N, \mathbf{R}_1)$ depends on the states of the first and the last DNA segments, and, in addition, on the potential energy of the last segment due to the force $f = |\mathbf{f}|$ applied to the DNA, see Equation (C5)–(C6) in Supplementary Appendix C.

To calculate all of the $\int d\mathbf{R}_j$ integrals in Equation (4), it is convenient to expand $T_{k_jk_{j+1}}(\mathbf{R}_j, \mathbf{R}_{j+1})$ and $\sigma_{k_Nk_1}(\mathbf{R}_N, \mathbf{R}_1)$ elements into the series of orthogonal D-functions, $D^s_{p,q}(\mathbf{R})$, that form basis in the Hilbert space of square-integrable functions defined on SO(3) group of 3D rotation matrices (83). Then by using orthogonality of $D^s_{p,q}(\mathbf{R})$ basis, it can be shown that $\int d\mathbf{R}_1 \ldots d\mathbf{R}_N$ integrals in Equation (4) reduce to a mere multiplication of matrices composed of the expansion coefficients of $T_{k_jk_{j+1}}(\mathbf{R}_j, \mathbf{R}_{j+1})$ and $\sigma_{k_Nk_1}(\mathbf{R}_N, \mathbf{R}_1)$ functions

[see Supplementary Appendix C]:

$$Z_{f,\tau} = \mathrm{Tr}\left(\mathbf{U}\mathbf{L}^{N-1}\mathbf{Y}\right) \quad (6)$$

Here the entries of matrix $\mathbf{L}$ are the expansion coefficients of $T_{k_j k_{j+1}}(\mathbf{R}_j, \mathbf{R}_{j+1})$ transfer-functions; and matrices $\mathbf{Y}$ and $\mathbf{U}$ are composed of the expansion coefficients of $\sigma_{k_N k_1}(\mathbf{R}_N, \mathbf{R}_1)$ functions, which for convenience reasons are split into two parts [see Supplementary Appendices C and F for more details].

Knowing the DNA partition function, $Z_{f,\tau}$, it is then rather straightforward to calculate the DNA extension (z) and linking number change (ΔLk) as well as the total number of protein-bound (N_{pr}) and bare (N_u) DNA segments in each of the states, u = L- or P-DNA, by differentiating $Z_{f,\tau}$ with respect to force (f), torque (τ), protein binding energy (μ_{pr}) or DNA base-pairing energy in the corresponding state (μ_n, $n = -1$ or -2), accordingly [see Equation (G1) in Supplementary Appendix G]. From these observables it is then easy to find the DNA superhelical density (σ) and the DNA occupancy fraction by DNA-bound proteins (O) as: $\sigma = \Delta\mathrm{Lk}/\mathrm{Lk}_0$ and $O = N_{\mathrm{pr}}/N$. Here Lk_0 is the linking number of a torsion-free B-DNA, which in the case of DNA comprised of N_{bp} base-pairs equals to $\mathrm{Lk}_0 = N_{\mathrm{bp}}/h_0$, where h_0 is the helical repeat of B-DNA.

Evaluation of the above parameters based on the transfer-matrix computations of the DNA partition function provides a simple and fast way to predict changes in the DNA conformation as well as in DNA–protein interactions in response to mechanical constraints applied to the DNA, making it possible to compare theoretical results presented here to direct measurements performed in single-molecule experiments.

DNA energy terms

As can be seen from the previous section, by having at hand a mathematical expression for the total conformational energy of DNA, it is possible to calculate the DNA partition function and predict the equilibrium behaviour of DNA under various force and torque constraints applied to it. To provide insights into the energy terms contributing to the total conformational energy of DNA, which were briefly mentioned in Equation (1), here we present their detailed mathematical description with references to Supplementary Appendices sections, where interested readers can find more additional information.

While E_{DNA} energy term in Equation (1) has been previously discussed in details in ref. (75), we would like to briefly remind that in the general case it has the following form:

$$E_{\mathrm{DNA}} = \sum_{j=1}^{N-1} \sum_{n,m=-2}^{0} \delta_{k_j n}\delta_{k_{j+1} m} \Big\{ \frac{a_n}{2}\left(\mathbf{R}_j\mathbf{z}_0 - \mathbf{R}_{j+1}\mathbf{z}_0\right)^2 + \frac{c_n}{2}\left[2\pi\,\Delta\mathrm{Tw}_j\left(\mathbf{R}_j, \mathbf{R}_{j+1}\right)\right]^2 + J\left(1-\delta_{nm}\right) \Big\} + q\sum_{j=1}^{N}\sum_{n=-2}^{0} \mu_n \delta_{k_j n} \quad (7)$$

Where δ_{nm} is the Kronecker delta ($\delta_{nm} = 1$ if $n = m$ and $\delta_{nm} = 0$, otherwise). $a_n = A_n/b_n$ and $c_n = C_n/b_n$ are dimensionless parameters describing the bending and twisting rigidities of bare DNA segments being state n ($n = 0$, -1 and -2 for B-, L- and P-DNA, respectively), where A_n, C_n and b_n are the bending and twisting persistence lengths of DNA, and the size of DNA segments in the respective state, accordingly (see Table 1). q is the number of base-pairs in each of the DNA segments, which is a fixed constant having the same value for all DNA segment states. μ_n is the base-paring energy of DNA in state n with respect to B-DNA form (see Table 1). J is the domain wall penalty that accounts for the cooperativity of DNA structural transitions, describing the molecule preference for structural uniformity (81,84). Finally, $\Delta\mathrm{Tw}_j(\mathbf{R}_j, \mathbf{R}_{j+1}) \approx \frac{1}{2\pi}\mathbf{R}_j\mathbf{z}_0 \cdot [\mathbf{R}_j\mathbf{x}_0 \times \mathbf{R}_{j+1}\mathbf{x}_0]$ is the local DNA twist between the jth and $(j+1)$th DNA segments.

From now on we will focus our attention on the last three energy terms, E_{protein}, Φ_f and Φ_τ, in Equation (1) that describe the elastic deformation energy of DNA caused by DNA–protein interactions and potential energies associated with the force and torque constraints applied to DNA. To calculate them, we generally need to know the DNA conformation inside nucleoprotein complexes formed on DNA. One of the main reasons for this is dependence of the DNA linking number change, ΔLk, on the global DNA conformation, which is determined by the relative orientations of all of the DNA segments, including those contributing to formation of nucleoprotein complexes. As a result, Φ_τ term generally depends on the nature of nucleoprotein complexes formed on DNA.

In the case of DNA-bending proteins, such as the one schematically shown in Figure 1D, the DNA linking number change associated with the formation of nucleoprotein complexes may vary in a wide range depending on the orientations of these complexes with respect to the rest of the DNA. Hence, one cannot assign a fixed linking number change to nucleoprotein complexes formed by DNA-bending proteins, and the relative orientations of all DNA segments inside such complexes must be known in order to calculate the above energy terms, which can be done, for example, by using existing X-ray crystallographic data for nucleoprotein complexes.

In contrast, nucleoprotein complexes formed by DNA-wrapping proteins [Figure 1E and F] make a well-defined fixed contribution, $\Delta\mathrm{Lk}_{\mathrm{pr}}$, to the DNA linking number change. Thus, one does not need to have exact information regarding the DNA conformation inside each of the nucleoprotein complexes to calculate the DNA linking number change. As a result, any such nucleoprotein complex can be replaced by a straight line connecting the entry and exit points of DNA, see Figure 1E and F. In this case, the DNA linking number change can be estimated by first calculating the contribution from all protein-unbound DNA segments, and then adding to it $\Delta\mathrm{Lk}_{\mathrm{pr}} \times M$ term, where M is total number of nucleoprotein complexes formed by DNA-wrapping proteins. Such approach greatly simplifies the final expression for the DNA partition function, making its computation much more easier in comparison to the DNA-bending proteins scenario described above.

However, it should be noted that while in the case of DNA-wrapping proteins the replaced DNA segments do

not make any contribution to the formula for the DNA total conformational energy, we still need to keep track of these segments by making a corresponding register shift by K DNA segments each time upon encountering one of the nucleoprotein complexes formed on DNA. One way to do this is to split the line connecting the entry and exit points of each nucleoprotein complex into K smaller subintervals, assigning each of these intervals to one of the replaced DNA segments. Thus, for example, if DNA segments with indexes $j, j+1, ..., j+K-1$ are bound to one of the DNA-wrapping proteins (such that $k_j = 1$, $k_{j+1} = 2$, ..., $k_{j+K-1} = K$) then we simply put: $\mathbf{R}_j = \mathbf{R}_{j+1} = ... = \mathbf{R}_{j+K-1} = \mathbf{R}_{\mathrm{pr,\,j}}$, where $\mathbf{R}_{\mathrm{pr,\,j}}$ is the rotation matrix describing the orientation of the line connecting the entry and exit points of the given nucleoprotein complex. In other words, all of the DNA segments taking part in the formation of a DNA-wrapping nucleoprotein complex can be assumed to have the same orientations, being aligned along a straight line connecting the entry and exit points of the complex, see Figure 1E and F.

Finally, we would like to note that in the special case of DNA-stiffening proteins that form straight filaments along DNA both of the above approaches lead to identical description of the resulting nucleoprotein complexes.

Following the above notes, it is not hard to obtain expressions for the DNA linking number change, ΔLk, as well as Φ_τ energy term by using a combination of the famous Călugăreanu-White's theorem (85,86) and the Fuller's approximate formula for the DNA writhe number (87). While the first states that ΔLk can be expressed as a sum of two components: $\Delta\mathrm{Lk} = \Delta\mathrm{Tw} + \mathrm{Wr}$, where $\Delta\mathrm{Tw} = \sum_{j=1}^{N-1} \Delta\mathrm{Tw}_j(\mathbf{R}_j, \mathbf{R}_{j+1})$ is the DNA total twist and Wr is the DNA writhe number; the second allows to express the DNA writhe number as a sum of local DNA segments' contributions, $\mathrm{Wr}^{\mathrm{F}} = \sum_{j=1}^{N-1} \mathrm{Wr}_j^{\mathrm{F}}(\mathbf{R}_j, \mathbf{R}_{j+1})$, where $\mathrm{Wr}_j^{\mathrm{F}}(\mathbf{R}_j, \mathbf{R}_{j+1}) = \frac{1}{2\pi}(\tilde{\alpha}_{j+1} - \tilde{\alpha}_j)(1 - \cos\beta_j)$, and $\tilde{\alpha}_{j+1}$ and $\tilde{\alpha}_j$ are the azimuthal Euler angles of the jth and $(j+1)$th DNA segments from the extended range of $(-\infty, +\infty)$ (75,88,89). The superscript F in the above equations indicates that the DNA writhe number calculation is based on the Fuller's formula approximation. The resulting mathematical expressions for the DNA linking number change in the presence of DNA interaction with different types of DNA-binding proteins can be found in Supplementary Appendix A.

Here we would like only to stress that the Fuller's formula provides correct estimations of the DNA linking number change for those DNA conformations which can be obtained by a continuous deformation of DNA initially extended along $\mathbf{z}_0$-axis direction in such a way that none of the DNA sections face the negative direction of $\mathbf{z}_0$-axis for any of the intermediate DNA configurations (87–89). A nearly straight DNA or DNA folded into a helical solenoid conformation are examples satisfying this criterion (88–91). In other cases, however, the DNA writhe number, Wr, does not necessarily equal to Wr^{F}. For this reason, the Fuller's formula works well only for DNA conformations that do not contain supercoiled plectoneme structures. Indeed, previous theoretical studies show that the Fuller's formula can be used to accurately predict the behaviour of DNA under a wide range of mechanical constraints up to the onset of the torque-induced buckling transition when DNA starts to develop supercoiled plectonemes (42,75,76,88–91).

More importantly, by utilizing the Fuller's approximation, it is possible to observe collapsing of bare DNA into compact conformations upon application of sufficiently large torques, which is accompanied by increase in the absolute value of the DNA linking number (75,76). Although the resulting conformations are not necessarily the same as supercoiled DNA plectonemes, the predicted force-extension curves of DNA subjected to torque constraints resemble those observed in single-molecule experiments, exhibiting very similar behaviour near the DNA buckling transition point, see ref. (75,76) and (52). Therefore, it is still possible to use the Fuller's approximation to describe the DNA supercoiling transition.

The only side-effect of such approach is that it leads to a slight shift of the predicted DNA supercoiling transition boundary relative to the experimentally measured position, which, however, can be easily corrected by adding a new term, $\delta\Phi_\tau$, to Φ_τ energy (i.e. $\Phi_\tau = -2\pi\tau\Delta\mathrm{Lk}^{\mathrm{F}} + \delta\Phi_\tau$). In the case of a structurally uniform DNA, this term simply equals to $\delta\Phi_\tau = \tau\lambda\mathrm{Wr}^{\mathrm{F}}$ with λ being a fixed scaling factor, see ref. (75,76). Whereas in a more realistic scenario when the DNA segments are allowed to make transitions between different structural states, the correction term takes somewhat sophisticated form as each of the DNA structures (B-, L- or P-DNA) is characterized by its own value of the scaling parameter, λ_n, see ref. (75,76) and Table 1:

$$\delta\Phi_\tau = \tau \sum_{j=1}^{N-1} \left[\sum_{n=-2}^{0} \delta_{k_j n}\lambda_n + \lambda_{\mathrm{pr}} \sum_{n=1}^{K} \delta_{k_j n} \right] \times \mathrm{Wr}_j^{\mathrm{F}}(\mathbf{R}_j, \mathbf{R}_{j+1}) \quad (8)$$

Here λ_n and λ_{pr} are scaling parameters associated with different DNA structures and DNA segments residing inside nucleoprotein complexes, respectively.

In this study, we consider only the proteins that bind to B-form DNA. As a result, in all our calculations we simply put $\lambda_{\mathrm{pr}} = \lambda_0$. Thus, in the above formula, λ_0 value is used for all of the vertices connecting neighbouring DNA segments inside nucleoprotein complexes.

The next energy term from Equation (1), Φ_f, has a very simple mathematical expression, which can be obtained by assuming that the global coordinate system $(\mathbf{x}_0, \mathbf{y}_0, \mathbf{z}_0)$ is aligned in such a way that its $\mathbf{z}_0$-axis faces in the direction of force $\mathbf{f}$ applied to the DNA. Then it is not hard to show that in this case Φ_f equals to:

$$\Phi_f = -\sum_{j=0}^{N} \sum_{n=-2}^{K} \delta_{k_j n} b_n f\left(\mathbf{z}_0 \cdot \mathbf{R}_j \mathbf{z}_0\right) \quad (9)$$

Here $f = |\mathbf{f}|$ is the force magnitude, and b_n is the size of DNA segments being in state n. Since in this study we consider only the proteins that bind to B-form DNA, the DNA segments constrained inside nucleoprotein complexes formed by DNA-bending or DNA-stiffening proteins should have approximately the same size as protein-unbound B-form DNA segments: $b_1 = ... = b_K = b_0$. As for DNA-wrapping proteins, since all of the DNA segments bound to such proteins are replaced by the lines connecting the entry and ex-

Table 1. Bare DNA parameters

DNA form	Bending persistence length, A_n (nm)	Twisting persistence length, C_n (nm)	Contour length relative to B-DNA form	DNA helical repeat, h_n (bp)	Base-pairing energy relative to B-DNA form, μ_n (k_BT)	λ_n
B-DNA	50 (55,108)	95 (56,93,109)	1	10.4 (110)	0	4.3 (75,76)
L-DNA	7 (80,82)	15 (80–82)	1.35 (80,82)	16 (56,80,81)	5.0 (75,76)	4.3 (75,76)
P-DNA	15 (82)	25 (82)	1.7 (77,78,82)	3 (56,77–80,82)	17.8 (75,76)	−0.5 (75,76)

To account for the cooperativity of the DNA structural transitions, the domain wall penalty, $J = 9.0\ k_BT$ (81,84), characterizing the DNA preference for structural uniformity was introduced into the transfer-matrix calculations in addition to the model parameters listed in the above table.

ist points of the resulting nucleoprotein complexes, with each line being subdivided into K equal intervals, we have: $b_1 = ... = b_K = r_{pr}/K$, where r_{pr} is the distance between the entry and exit points of the nucleoprotein complexes.

Finally, $E_{protein}$ energy term from Equation (1) equals to the sum of individual nucleoprotein complexes' energies, which include: (i) the protein binding energy to DNA, μ_{pr}, and (ii) the DNA elastic deformation energies at the entry and exit points of the nucleoprotein complex, E_{in} and E_{out}, respectively. Thus, denoting the orientations of the DNA segments sitting next to the entry and exit points of a nucleoprotein complex by rotation matrices $\mathbf{R}_{in}$ and $\mathbf{R}_{out}$, and orientations of the first and the last DNA segments in the nucleoprotein complex by rotation matrices $\mathbf{R}_{first}$ and $\mathbf{R}_{last}$ [see Figure 1C and D], the energy of each nucleoprotein complex can be written in the following form:

$$E_{pr} = -\mu_{pr} + E_{in}(\mathbf{R}_{in}, \mathbf{R}_{first}) + E_{out}(\mathbf{R}_{last}, \mathbf{R}_{out}) \quad (10)$$

Where in the case of DNA-wrapping proteins $\mathbf{R}_{first} = \mathbf{R}_{last} = \mathbf{R}_{pr}$, see Figure 1E and F. As for E_{in} and E_{out} terms describing the DNA elastic deformation energies at the entry and exit points of a nucleoprotein complex, in the general case they equal to:

$$E_{in}(\mathbf{R}_{in}, \mathbf{R}_{first}) = \frac{a_{pr}}{2}(\mathbf{R}_{in}\mathbf{A}_{in}\mathbf{z}_0 - \mathbf{R}_{first}\mathbf{z}_0)^2 + \frac{c_{pr}}{2}[2\pi\,\Delta\mathrm{Tw}(\mathbf{R}_{in}\mathbf{A}_{in}, \mathbf{R}_{first})]^2 \quad (11)$$

and

$$E_{out}(\mathbf{R}_{last}, \mathbf{R}_{out}) = \frac{a_{pr}}{2}(\mathbf{R}_{last}\mathbf{A}_{out}\mathbf{z}_0 - \mathbf{R}_{out}\mathbf{z}_0)^2 + \frac{c_{pr}}{2}[2\pi\,\Delta\mathrm{Tw}(\mathbf{R}_{last}\mathbf{A}_{out}, \mathbf{R}_{out})]^2 \quad (12)$$

Here, a_{pr} and c_{pr} are dimensionless bending and twisting elasticities of the entry and exit DNA segments of the nucleoprotein complex; $\mathbf{A}_{in}$ and $\mathbf{A}_{out}$ are two rotation matrices that determine the equilibrium orientations of the entry and exit DNA segments relative to the core part of the nucleoprotein complex such that in mechanical equilibrium we have: $\mathbf{R}_{in}^{(eq)}\mathbf{A}_{in} = \mathbf{R}_{first}^{(eq)}$ and $\mathbf{R}_{last}^{(eq)}\mathbf{A}_{out} = \mathbf{R}_{out}^{(eq)}$. Finally, $2\pi\,\Delta\mathrm{Tw}(\mathbf{R}_{in}\mathbf{A}_{in}, \mathbf{R}_{first})$ and $2\pi\,\Delta\mathrm{Tw}(\mathbf{R}_{last}\mathbf{A}_{out}, \mathbf{R}_{out})$ are the twist angles of the entry and exit DNA segments with respect to their equilibrium orientations.

Specifically, in the case of a DNA-stiffening protein that forms straight nucleoprotein filaments along the DNA, we have: $a_{pr} = A_{pr}/(b_0K)$ and $c_{pr} = C_{pr}/(b_0K)$, where A_{pr} and C_{pr} are the bending and twisting persistence lengths of protein-covered DNA, and K is the number of DNA segments bound to a single protein. Furthermore, for such a protein $\mathbf{A}_{in} = \mathbf{A}_{out} = \mathbf{I}$, where $\mathbf{I}$ is the identity matrix. As a result, in mechanical equilibrium all of the rotation matrices describing orientations of the protein-bound DNA segments have identical values: $\mathbf{R}_{in}^{(eq)} = \mathbf{R}_{first}^{(eq)} = ... = \mathbf{R}_{last}^{(eq)} = \mathbf{R}_{out}^{(eq)}$ (i.e. protein forms straight filaments).

Additional details regarding the mathematical description of the nucleoprotein complexes' contribution into the total conformational energy of DNA can be found in Supplementary Appendix B.

Finally, it should be noted that in all of the calculations presented below, the size of the DNA segments was set to be equal to $q = 1.5$ bp for all of the DNA structural states and the DNA length was ∼4.7 kbp (a total of $N = 3073$ segments in the discretized polymer chain representing DNA). The values of the rest of the model parameters are listed in Table 1 (for bare DNA segments) and Table 2 (for different types of nucleoprotein complexes).

Main assumptions of the theory

In this section we would like to summarize all of the main assumptions used to derived Equation (6) for the partition function of DNA interacting with proteins, which is important for understanding of potential applications that can be solved using the transfer-matrix formalism described above.

First of all, in order to derive mathematical formulas for the elements of the DNA transfer-matrix, $\mathbf{L}$, in this study it was assumed that nucleoprotein complexes have fixed 3D structures, see Supplementary Appendices B–F. Therefore, application of the current theoretical framework should be restricted mainly to DNA–protein assemblies that have a well-defined conformation. While this assumption serves as a good first level of approximation to the description of DNA interaction with many different types of proteins, it should be noted that some nucleoprotein complexes may be very flexible, possessing more than one stable conformation. In this case, the formulas presented in this study should be accordingly modified to accurately depict force- and torque-dependent behaviour of such complexes.

Furthermore, the above assumption of a fixed nucleoprotein complex structure implies that the current model does not take into consideration cases of partial proteins binding to DNA, which may take place under sufficiently strong forces and torques applied to DNA. For instance, existing experimental data show that at 2–3 pN force, the outer turn of DNA interacting with histone octamers can be unwrapped from nucleosome complexes, while the inner

Table 2. Values of the model parameters for different nucleoprotein complexes studied in this work, which were used in the transfer-matrix calculations.

Protein	Bending rigidity, a_{pr}	Twisting rigidity, c_{pr}	Binding energy to DNA, μ_{pr} ($k_B T$)	Cooperative binding energy, J_{pr} ($k_B T$)	Linking number change, ΔLk_{pr}	$\mathbf{A}_{in}$, $\mathbf{A}_{out}$, $\mathbf{A}_{ht}$ and $\mathbf{A}_j$ Euler rotation matrices
DNA-stiffening	33.3	33.3	3.0	2.0	N/A	$\mathbf{A}_{in} = \mathbf{A}_{out} = \mathbf{A}_{ht} =$ $= \mathbf{A}_j = \mathbf{I}(0, 0, 0)$
DNA-bending	33.3	33.3	2.0	0.0	N/A	$\mathbf{A}_{in} = \mathbf{A}_{out} = \mathbf{A}_1 =$ $= \mathbf{I}(0, 0, 0)$ $\mathbf{A}_2(\pi, 0.2, \pi)$
Nucleosomes	33.3	33.3	40.0	0.0	−1.2	$\mathbf{A}_{in}(0, 2.12, -0.79)$ $\mathbf{A}_{out}(-0.79, 2.12, 0)$ $\mathbf{A}_j = \mathbf{I}(0, 0, 0)$
L-tetrasomes	33.3	33.3	26.3	0.0	−0.73	$\mathbf{A}_{in,\,L}(0, 2.26, -1.11)$ $\mathbf{A}_{out,\,L}(-1.11, 2.26, 0)$ $\mathbf{A}_j = \mathbf{I}(0, 0, 0)$
R-tetrasomes	33.3	33.3	24.0	0.0	+1.0	$\mathbf{A}_{in,\,R}(0, 2.26, 1.11)$ $\mathbf{A}_{out,\,R}(1.11, 2.26, 0)$ $\mathbf{A}_j = \mathbf{I}(0, 0, 0)$

Matrices $\mathbf{A}_j$ in the last column of the table describe the relative orientations of DNA segments inside the respective nucleoprotein complexes, see Supplementary Appendix B and Appendices F1–F3 for more details.

turn remains stably attached to the protein core, resulting in a partially bound state of histone octamers to a mechanically stretched DNA (43).

However, despite the above limitations, it is very easy to make necessary modifications to the theory in order to incorporate into the model partial binding of proteins to DNA and multiple conformations of nucleoprotein complexes formed by flexible proteins. This can be achieved simply by adding new DNA segment states and/or new elements into the DNA transfer-matrix in the same way as it has been done in the case of DNA interaction with histone tetramers that can flip between the two alternative conformations, see more details in DNA-wrapping proteins section ('Results' section), Supplementary Appendix F3 and at the end of Appendix G.

The next assumption that has been used in our derivations is the propensity of DNA-binding proteins to form nucleoprotein complexes only on B-form DNA. While there is not much information regarding the proteins' abilities to bind to alternative DNA structures, such as L- or P-DNA, it should be noted that it will be rather straightforward to include newly discovered protein–L-DNA and protein–P-DNA complexes into the transfer-matrix calculations again by introducing additional DNA segment states into the model.

Finally, to minimize the formulas' complexity, in this study we have not considered in detail the DNA and proteins' volume exclusion effect. As a result, the current theory cannot be applied to scenarios in which the volume exclusion plays a dominant role in determining the global DNA conformation. However, in principle, it is still possible to include such an effect in a mathematically rigorous way into the transfer-matrix formalism by making use of Hubbard–Stratonovich transformation that results in addition of an auxiliary fluctuating field to the DNA total conformational energy, see ref. (92) for details.

In addition to the above assumptions, we also used in this work the Fuller's approximate formula for the calculation of the DNA writhe number, see the previous section. From the existing theoretical studies, it is known that by utilizing this formula it is possible to obtain rather accurate estimations of the DNA linking number change for the most of DNA conformations up to the buckling transition point when DNA starts to develop supercoiled plectonemes (75,76,87–89). However, as soon as plectonemes start to appear in DNA, the Fuller's formula fails to provide correct values for the DNA writhe number, which restricts application of the transfer-matrix formalism up to the buckling transition point.

Nevertheless, as has been shown in our previous studies (75,76), it is still possible to use the transfer-matrix calculations to predict transition boundaries between different structural states of DNA, including the torque-induced change between the extended and supercoiled DNA conformations. Furthermore, since binding of DNA-bending and DNA-wrapping proteins to DNA results in formation of solenoid-like complexes for which the Fuller's formula works rather well (88,89), it is likely that the transfer-matrix formalism also can be used to obtain accurate predictions regarding the behaviour of DNA compacted by these types of proteins under force and torque constraints. This broadens application of the transfer-matrix theory to many interesting DNA–protein interaction scenarios, which are frequently studied in single-molecule experiments.

RESULTS

Mechanical response of bare DNA to force and torque constraints

Using the above transfer-matrix approach, we first investigated the effects of force and torque constraints on the conformation of bare DNA and its transition between different

structural states, such as B-, L- and P-DNA, in the absence of DNA-binding proteins in solution.

It should be noted that although the case of bare DNA has been discussed in detail in our previous studies (75,76), it is used in this work as a control against which all other scenarios describing DNA interactions with proteins are compared. For this reason, we briefly recall in this section what is known about behaviour of a mechanically stretched and twisted bare DNA.

By substituting the values of the model parameters listed in Table 1 that describe the physical properties of bare DNA into Equation (6), it is not hard to obtain the DNA force-extension curves, $z(f)|_{\tau=\tau_0}$ and force-superhelical density curves, $\sigma(f)|_{\tau=\tau_0}$, at various torque constraints ($\tau = \tau_0$), which are shown in Figure 2A. The top and the bottom panels of Figure 2A demonstrate the force-extension and force-superhelical density curves for the case of negative ($\tau < 0$ pN·nm) and positive torques ($\tau > 0$ pN·nm), respectively.

From the graphs, it can be seen that the mechanical response of bare DNA to the applied force and torque constraints is highly non-linear. While at small torques ($-5 \leq \tau \leq 5$ pN·nm) the DNA force-extension curves do not deviate much from the one corresponding to a torsionally relaxed DNA ($\tau = 0$ pN·nm), application of stronger torsional stress ($|\tau| > 5$ pN·nm) results in rapid decrease of the DNA extension as soon as the stretching forces, f, drops below a certain threshold value, see Figure 2A, left top and bottom panels. Calculations of the DNA superhelical density, $\sigma = \Delta Lk/Lk_0$, as a function of the applied force and torque constraints show that such torque-induced DNA collapsing is accompanied by a simultaneous steep change of the DNA superhelical density [Figure 2A, right top and bottom panels], resembling typical behaviour of strongly twisted DNA that undergoes transition into a compact supercoiled conformation, which is typically observed in single-DNA manipulation experiments (52).

Furthermore, from the left panel of Figure 2B showing the DNA torque-extension curves, $z(\tau)|_{f=f_0}$, calculated at various force constraints ($f = f_0$), it can be seen that the DNA folding into the supercoiled conformation occurs both at positive and negative torques in a symmetric manner at low stretching forces ($f < 0.5$ pN). However, at larger forces ($f \geq 0.5 - 0.7$ pN) this symmetry breaks as stronger stretching makes it harder for DNA to form compact supercoiled structures; thus, preventing release of the accumulated DNA elastic twist energy via the DNA supercoiling process. As a result, transition of DNA from B-form into alternative L- and P-DNA structures becomes a more energetically favourable way for the DNA twist elastic energy relaxation at large stretching forces ($f \geq 0.5$ pN).

It is not hard to see the effects of these DNA structural transitions on the left panel of Figure 2B as they manifest themselves in an abrupt change of the twist-extension curves' behaviour. For example, at forces $f \geq 5$ pN and large negative torques ($\tau < -11$ pN·nm) the DNA extension increases by ∼1.1–1.3 times comparing to the case of a torsionally relaxed B-DNA ($\tau = 0$ pN·nm), indicating DNA transition into alternative L-DNA form, which is accompanied by a simultaneous DNA superhelical density drop to the value of $\sigma \sim -2.0$—see the right panel in Figure 2B showing the DNA torque-superhelical density curves, $\sigma(\tau)|_{f=f_0}$, calculated at various force constraints. Likewise, at high positive torques ($\tau > 35$ pN·nm) the DNA extension becomes ∼1.6 times longer than that of a torsionally relaxed DNA ($\tau = 0$ pN·nm), designating the DNA transition into P-DNA state, which is accompanied by a simultaneous large DNA superhelical density increase to the value of $\sigma \sim 3.0$, see the right panel in Figure 2B.

Similarly to B-DNA, both L- and P-DNA experience buckling transition from the extended to a compact supercoiled conformation, which is indicated on the left panel of Figure 2B by steep decrease of the DNA extension at large negative and positive torques as soon as the applied force drops below a certain threshold, whose value is slightly larger for L-DNA (∼1.5 pN) as compared to the B-DNA case and even more higher for P-DNA (∼20 pN) due to higher elasticities of L- and P-DNA forms.

Altogether, the above results demonstrate that the global conformation and structure of bare DNA are highly sensitive to mechanical constraints applied to it, in good agreement with the existing experimental data previously reported in multiple single-molecule studies (56,58,77,79–81,93).

Effects of DNA-stiffening proteins on the DNA mechanical response to force and torque constraints

Next, we used the transfer-matrix formalism to investigate the effects of force and torque constraints on DNA interaction with DNA-stiffening proteins, which upon binding to DNA form rigid nucleoprotein filaments that increase the DNA bending persistence lengths, and presumably the DNA twisting rigidity (27,29,31,33,94–98). For this purpose, we carried out calculations in which the bending and twisting persistence lengths of protein-covered DNA were set to $A_{pr} = 200$ nm and $C_{pr} = 200$ nm, respectively, with the value of the bending persistence length, A_{pr}, falling in the range of 100 nm $< A_{pr} <$ 500 nm previously reported for different types of DNA-stiffening proteins (27,29,31,33,94–98).

In the calculations, the proteins were allowed to bind to any place on the DNA as soon as the corresponding DNA section was in B-form (i.e. proteins interact only with B-form DNA), and each DNA-bound protein was assumed to occupy $K = 12$ DNA segments [∼18 bp, see schematic Figure 1C], which is a typical DNA binding site size for many known DNA-stiffening proteins. Having at hand the bending and twisting persistence lengths of protein-covered DNA, and the binding site size of the proteins, it is then straightforward to find the values of dimensionless bending and twisting elasticities of the entry and exit DNA segments of nucleoprotein complexes: $a_{pr} = A_{pr}/(Kb_0) = c_{pr} = C_{pr}/(Kb_0) = 33.3$ (see Table 2), which were used in all of the computations presented below.

Finally, formation of nucleoprotein complexes on DNA was associated with the DNA–protein interaction energy of $\mu_{pr} = 3.0\ k_BT$. In addition, since it is known that DNA-stiffening proteins often assemble into nucleoprotein filaments on DNA through cooperative interaction with each other (27,29,31,33,94–98), a cooperative binding energy of $J_{pr} = 2.0\ k_BT$ between proteins occupying neighbouring

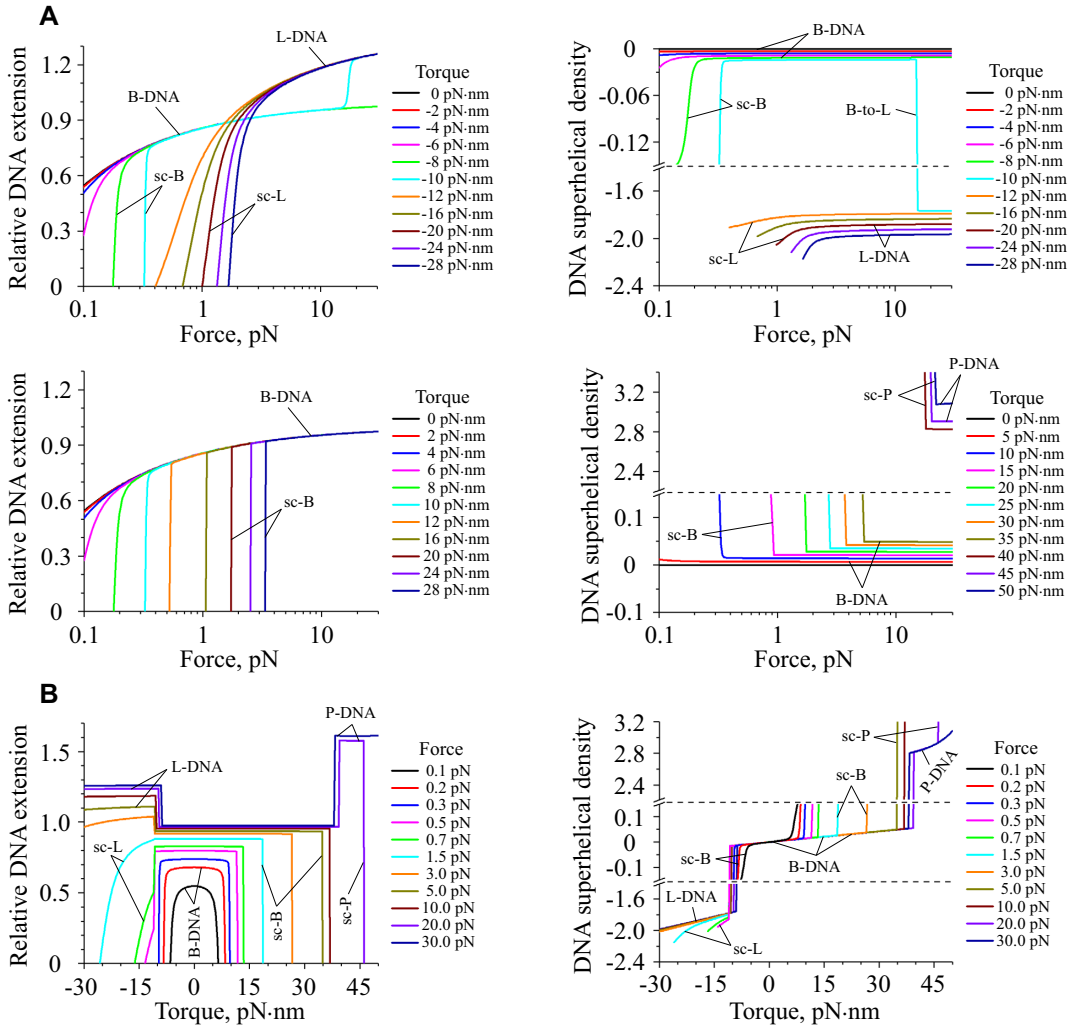

Figure 2. Mechanical response of bare DNA to the applied force and torque constraints in the absence of DNA-binding proteins. The figure shows (**A**) force-extension $[z(f)|_{\tau=\tau_0}]$ and force-superhelical density curves $[\sigma(f)|_{\tau=\tau_0}]$ as well as (**B**) torque-extension $[z(\tau)|_{f=f_0}]$ and torque-superhelical density curves $[\sigma(\tau)|_{f=f_0}]$ obtained at different values of the force, f, and torque, τ, exerted to the DNA. From panel (A), it can be seen that application of a sufficiently large torque ($|\tau| \geq 6$ pN·nm) leads to collapsing of bare DNA, which is accompanied by development of supercoiled DNA structures. Panel (B) provides additional details, showing that at forces $f < 0.5$ pN all of the torque-extension curves have symmetric profiles with respect to both positive and negative torques, while at larger forces of $f \sim 0.5 - 0.7$ pN this symmetry breaks due to B-DNA switching into alternative L- and P-DNA structures, which results in the respective change of the DNA superhelical density. In all panels, the DNA extension is normalized to the total contour length of DNA in B-form. Abbreviations sc-B, sc-L and sc-P are used to indicate supercoiled states of B-, L- and P-DNA, respectively.

DNA binding sites was introduced into the transfer-matrix calculations.

After substituting the above model parameters into the transfer-matrix, **L**, and boundary condition matrix, **Y**, describing DNA interaction with DNA-stiffening proteins [see Equation (F6) in Supplementary Appendix F1], we found the values of the observables, such as the DNA extension and superhelical density, in order to investigate a potential role of DNA-stiffening proteins in modulation of the DNA conformation under force and torque constraints. The final results of the computations are shown in Figure 3 and Supplementary Figure S1.

From the direct comparison between the force-extension curves calculated for bare DNA (dotted lines) and protein-covered DNA (solid lines) displayed in the left panels of Figure 3A, it can be seen that formation of rigid nucleoprotein filaments on DNA, as expected, results in increased extension of a torsionally relaxed DNA at low forces ($f \sim 0.1$ pN) due to the higher bending persistence length of the protein-covered DNA. In addition, the force-extension curves of protein-bound DNA demonstrate rather substantial shift in their buckling transition point at which DNA starts to collapse into a compact conformation towards lower values of the applied stretching force. This result indicates that nucleoprotein filaments assembled on DNA can delay or even completely inhibit development of supercoiled DNA structures. Indeed, the force-superhelical density curves of protein-covered DNA exhibit very similar shifts towards the lower values of the stretching force, validating that DNA interaction with DNA-stiffening proteins has an adverse effect on the formation of supercoiled DNA structures, see the right panels in Figure 3A.

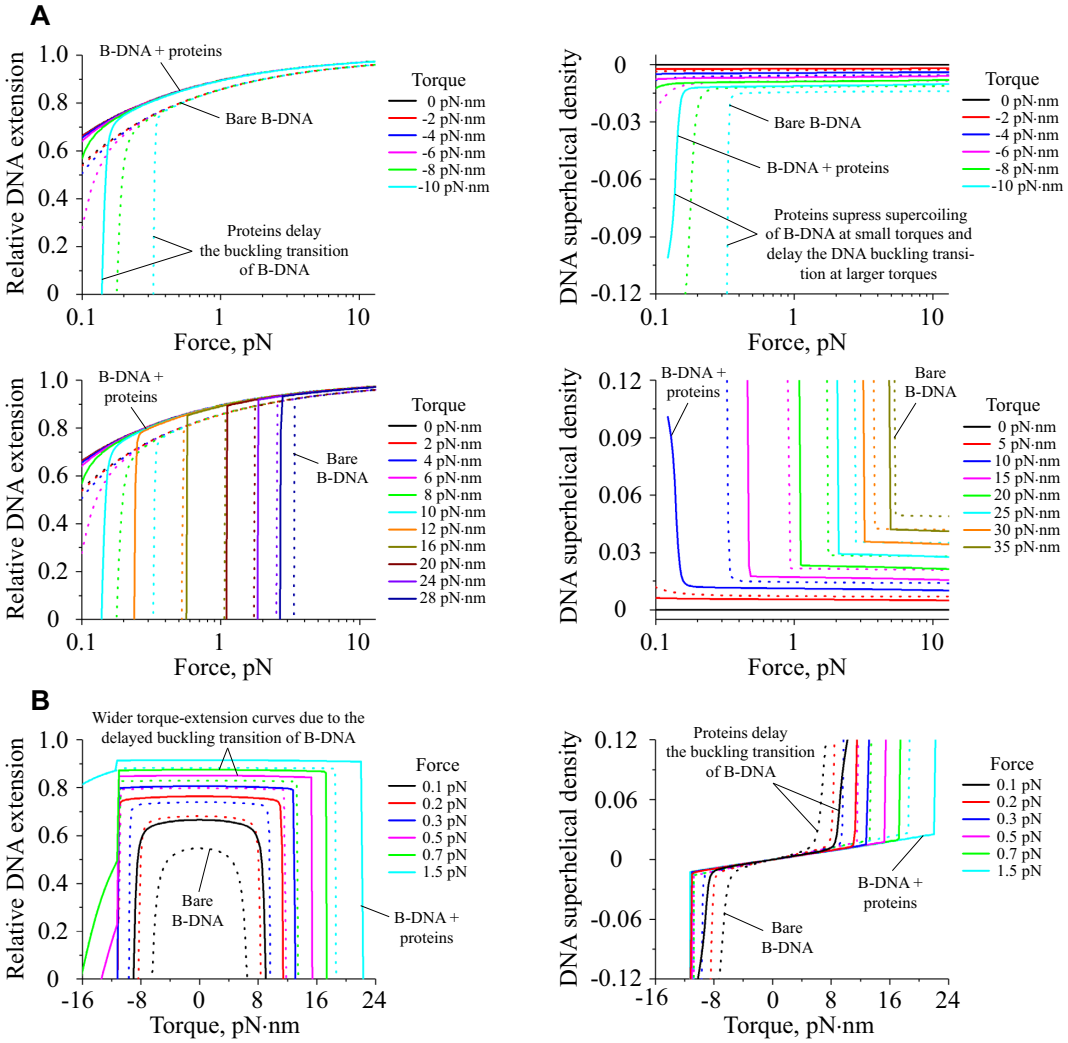

Figure 3. Mechanical response of DNA to the applied force and torque constraints in the presence of DNA interactions with DNA-stiffening proteins. The figure shows (**A**) force-extension and force-superhelical density curves obtained at different values of the torque, τ, as well as (**B**) torque-extension and torque-superhelical density curves obtained at different values of the force, f, exerted to the DNA. Solid curves demonstrate the behaviour of DNA in the presence of nucleoprotein complexes formation by DNA-stiffening proteins; whereas, dotted curves indicate mechanical response of bare DNA under the same force and torque constraints. As can be seen from comparison between the force-extension and force-superhelical density curves calculated for protein-covered and bare DNA, formation of rigid nucleoprotein filaments by DNA-stiffening proteins results in either complete disappearance or leftward shift of the DNA buckling transition point to smaller values of the applied force, indicating delay in the formation of supercoiled DNA structures. Such protein-induced suppression of the DNA supercoiling can be also clearly observed from the widening of the torque-extension and torque-superhelical density curves in the presence of DNA interactions with DNA-stiffening proteins in comparison to the case of bare DNA. In all panels, the DNA extension is normalized to the total contour length of DNA in B-form.

Such DNA behaviour can be easily understood by recalling that DNA folding into compact supercoiled structures is initiated by DNA buckling—formation of initial DNA loops, which eventually develop into supercoiled DNA plectonemes. Since this process requires DNA bending at the buckling site, it is clear that DNA-stiffening nucleoprotein filaments will be preventing formation of such DNA loops unless the applied torsional stress is sufficiently high to overcome the nucleoprotein filaments' resistance to the bending. As a result, onset of the DNA supercoiling transition will be delayed in the presence of DNA-stiffening proteins in solution.

The torque-extension curves shown on the left panels of Figure 3B and Supplementary Figure S1b provide further details regarding the effect of stiff nucleoprotein filaments onto the global conformation of DNA, demonstrating that the most significant changes, such as delay in the DNA buckling transition that results in widening of the torque-extension curves, take place mainly at low forces ($f \leq 3$ pN); whereas at higher forces the mechanical response of the protein-covered DNA to force and torque constraints is practically identical to that of a bare DNA in the absence of proteins in solution [compare the left panels of Figure 2B and Supplementary Figure S1b].

Interestingly, from the left and right panels of Figure 2B and Supplementary Figure S1b it can be seen that binding of DNA-stiffening proteins to DNA has practically negligible suppressing effect on the DNA transitions from B- to

L- or P-DNA forms. The main reason for this is that the average binding energy of the proteins to DNA per single base-pair (<1 k_BT) is much lower than the free energies μ_u (u = L or P) associated with the DNA transitions between different structural states ($\mu_u \sim 3 - 20\ k_BT$ per base-pair, see Table 1). As a result, this does not allow proteins to efficiently interfere with the DNA structural transitions unless the protein binding energy to DNA is very high.

In addition to the above curves characterizing the DNA behaviour under mechanical constraints in the presence of DNA-stiffening protein, we also calculated the average DNA occupancy fraction by proteins as a function of the force and torque applied to the DNA, see Supplementary Figure S5a. As expected for $\mu_{pr} = 3.0\ k_BT$ binding energy and $J_{pr} = 2.0\ k_BT$ cooperative binding energy of proteins to DNA used in the calculations, a large part of the DNA is occupied by nucleoprotein complexes. Nevertheless, previously reported phenomenon of enhancement of the protein binding to DNA with increase in the stretching force exerted on the DNA (42) still can be clearly seen on all of the panels in Supplementary Figure S5a. In contrast to the stretching force, application of stronger torsional stress to DNA promotes proteins dissociation from it, see the middle and right panels of Supplementary Figure S5a. Development of supercoiled DNA structures at low forces ($f \leq 3$ pN) and high torques ($\tau > 10$ pN·nm) further destabilizes nucleoprotein complexes formed on DNA by DNA-stiffening proteins, resulting in dramatic decrease of the DNA occupancy fraction.

Such unusual behaviour of DNA-stiffening proteins is tightly related to the changes in the DNA entropic elasticity taking place upon proteins interaction with DNA. Namely, formation of stiff nucleoprotein filaments leads to restriction of available conformations that can be taken by protein-covered DNA. As a result, there exists an entropic penalty for the binding of DNA-stiffening proteins to DNA at low forces at which DNA tends to assume more coiled conformations. On the other hand, application of stronger tension to DNA leads to a more extended DNA conformation, resulting in reduction of the entropic penalty associated with the proteins' DNA-stiffening effect. Thus, in general, mechanical stretching of DNA promotes formation of nucleoprotein filaments by DNA-stiffening proteins.

As for the role of torque in regulation of the DNA-stiffening proteins' affinity to DNA, it is clear that rigid nucleoprotein filaments have smaller propensity to twist under applied torsional stress. This leads to a smaller change in the total DNA linking number in the case of protein-covered DNA comparing to the case of bare DNA. Thus, the potential energy associated with the DNA twisting will be smaller for bare DNA than for protein-covered DNA, suggesting that nucleoprotein complexes will be losing their stability under the applied torque. Eventually, this will result in partial dissociation of DNA-stiffening proteins from DNA.

At the buckling transition point, proteins interaction with DNA is further compromised by the DNA bending into loops that prevent formation of extended nucleoprotein filaments by DNA-stiffening proteins. This leads to apparent reduction of the proteins' binding affinity to DNA, which is manifested by the drop in the DNA occupancy fraction curves shown in the middle and right panels of Supplementary Figure S5a at the DNA buckling transition point.

Effects of DNA-bending proteins on the DNA mechanical response to force and torque constraints

We further investigated the effects of force and torque constraints on the DNA-binding properties of DNA-bending proteins and explored the role of this type of proteins in regulation of the global DNA conformation. As a classical example of a DNA-bending protein, we used *Escherichia coli* integration host factor (IHF) as a model DNA-architectural protein in the transfer-matrix calculations, which is known to introduce sharp DNA bending at its binding site (22).

Following the existing structural and single-molecule data for IHF–DNA nucleoprotein complexes, the binding site size of IHF was set to 36 bp (i.e. $K = 24$ DNA segments) in all our computations, with the bending angle of DNA due to formation of the nucleoprotein complex being 150°, see schematic Figure 1D and ref. (22,32). As in the case of DNA-stiffening proteins, in this section we assumed that IHF binds only to B-form DNA. To reproduce the experimentally measured detachment force at which IHF dissociates from DNA [~0.8 pN (32)], the IHF binding energy to DNA was put equal to $\mu_{pr} = 2.0\ k_BT$. For the simplicity of calculations, in this study we did not consider the sequence-dependent affinity of IHF to DNA. As for the effective bending and twisting rigidities of IHF-DNA nucleoprotein complexes, a_{pr} and c_{pr}, we used the same values for these model parameters as in the case of DNA-stiffening proteins described in the previous section, see Table 2.

Substituting the above parameters into Equation (F9)–(F10) in Supplementary Appendix F2 that describe the transfer-matrix, **L**, and boundary condition matrices, **Y** and **U**, of DNA interacting with IHF proteins, we plotted the force- and torque-extension curves [$z(f)|_{\tau=\tau_0}$ and $z(\tau)|_{f=f_0}$] as well as the force- and torque-superhelical density curves of DNA [$\sigma(f)|_{\tau=\tau_0}$ and $\sigma(\tau)|_{f=f_0}$] at various force ($f = f_0$) and torque ($\tau = \tau_0$) constraints, see Figure 4 and Supplementary Figure S2.

The first obvious change in the conformation of DNA, which can be clearly seen from the force-extension curves calculated for protein-covered DNA (solid lines) shown in the left top and bottom panels of Figure 4A, is collapsing of DNA into a compact conformation due to its interaction with IHF proteins that takes place at forces below 1 pN in a wide range of the applied torque constraints ($-11 \leq \tau \leq 12$ pN·nm). This is in stark contrast to the behaviour of bare DNA (dotted lines), which either stays in the extended conformation (at $-6 \leq \tau \leq 6$ pN·nm torques) or undergoes supercoiling (at $|\tau| \geq 6$ pN·nm torques), but only at considerably smaller forces than in the case of IHF-covered DNA.

Interestingly, the force-superhelical density curves of DNA interacting with IHF proteins reveal that application of even small torsional stress to the DNA ($|\tau| \leq 5$ pN·nm) leads to development of supercoiled DNA conformations of the same sign as the applied torque [solid lines in the right top and bottom panels of Figure 4A], which is again in sharp contrast to the bare DNA case where the

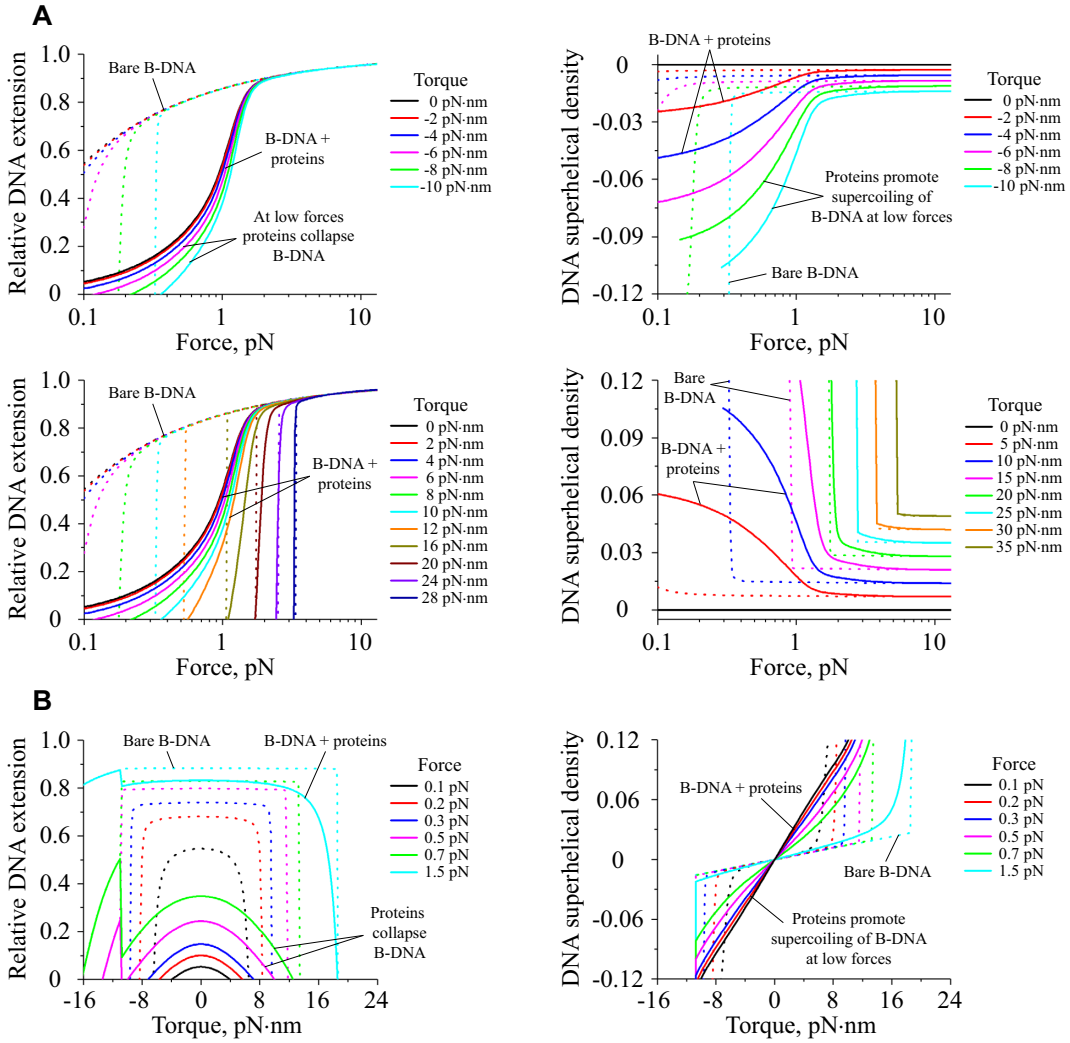

Figure 4. Mechanical response of DNA to the applied force and torque constraints in the presence of DNA interactions with DNA-bending proteins. The figure shows (**A**) force-extension and force-superhelical density curves obtained at different values of the torque, τ, as well as (**B**) torque-extension and torque-superhelical density curves obtained at different values of the force, f, exerted to the DNA. Solid curves demonstrate the behaviour of DNA in the presence of nucleoprotein complexes formation by DNA-bending protein; whereas, dotted curves indicate mechanical response of bare DNA under the same force and torque constraints. From panel (A), it can be seen that formation of nucleoprotein complexes by DNA-bending proteins results in DNA compaction at small forces ($f < 1$ pN), which is accompanied by a gradual increase in the magnitude of the DNA superhelical density that assumes either negative or positive sign depending on the direction of the applied torque. The left panel (B) provides further details, demonstrating that while having more compact shapes, the DNA torque-extension curves maintain their symmetry with respect to the torque sign up to the point where DNA experiences transition into alternative L-DNA structure at $\tau \sim -11$ pN·nm, indicating that formed nucleoprotein complexes do not discriminate between positive or negative torques applied to the DNA. In all panels, the DNA extension is normalized to the total contour length of DNA in B-form.

superhelical density remains near zero in the same torque range (dotted lines in the same panels). This result indicates that although the IHF-mediated DNA bending does not have a preferential chirality at zero torque, it readily assumes left-handed/right-handed conformation in response to negative/positive torques applied to the DNA, suggesting that nucleoprotein complexes formed by IHF can easily flip between left- and right-handed structures.

Furthermore, as can be seen from the right panels of Figure 4A, the magnitude of the superhelical density of IHF-covered DNA experiences rather moderate increase with reducing stretching force in $\tau \in [-11, -6]$ and $\tau \in [6, 11]$ pN·nm torque ranges. At the same time, bare DNA rapidly develops supercoils at these conditions, which result in the steep DNA superhelical density change. Thus, it can be concluded that IHF remains stably bound to DNA in this torque range, suppressing formation of supercoiled bare DNA structures that otherwise would form at forces $f <$ 1 pN. Indeed, the DNA occupancy fraction curves shown in the left and middle panels of Supplementary Figure S5b demonstrate that the amount of DNA-bound IHF proteins stay at a constant level at low forces ($f < 1$ pN) in the broad range of the applied torque constraints ($-11 \leq \tau \leq$ 12 pN·nm).

Application of stronger positive torques ($\tau \geq 12$ pN·nm) leads to the shift of the DNA occupancy fraction curves to higher force values, suggesting torque-induced stabilization of nucleoprotein complexes formed by IHF proteins,

see the middle panel of Supplementary Figure S5b. However, due to the failure of the Fuller's formula to describe the DNA writhe number beyond the buckling transition point, which results in potentially inaccurate prediction of the DNA occupancy fraction by the transfer-matrix calculations for strongly supercoiled DNA, it is not clear whether or not the DNA occupancy fraction curves eventually reach the same maximum level at $\tau \geq 12$ pN·nm torques as in the case of lower torque values ($-11 \leq \tau \leq 12$ pN·nm). Although, resemblance of the force-extension and force-superhelical density curves of IHF-covered DNA to those of bare DNA [Figure 4A] suggests that IHF may partially dissociate from DNA at $\tau \geq 12$ pN·nm torques due to the formation of supercoiled bare DNA structures, similarly to the case of DNA-stiffening proteins described in the previous section.

Torque-extension curves shown in the left panels of Figure 4B and Supplementary Figure S2b provide further details regarding the role of IHF proteins in force- and torque-dependent regulation of the DNA conformation. Namely, by comparing the results presented in the left panels of Figure 2B and Supplementary Figure S2b, it can be seen that at high forces ($f \geq 3$ pN) the torque-extension curves of DNA interacting with IHF proteins are identical to those of bare DNA, indicating that IHF binding to DNA is inhibited in this force range regardless of the magnitude of the applied torque, in full accordance with the torque-DNA occupancy fraction graphs plotted in the right panel of Supplementary Figure S5b. At lower forces ($f \leq 1.5$ pN), however, formation of nucleoprotein complexes on DNA by IHF proteins leads to a very drastic change in the DNA conformation—the DNA extension becomes significantly shorter than that of bare DNA due to the DNA bending by IHF proteins,—see the left panels of Figure 2B and Supplementary Figure S2b, and also the left panel of Figure 4B that displays the torque-extension curves of protein-covered DNA (solid lines) and bare DNA (dotted lines) on the same graph.

Application of torques from $\tau \in [-11, 12]$ pN·nm range leads to further DNA extension drop with the rising torque magnitude, indicating increase in the IHF binding affinity to DNA and formation of more compact DNA–protein structures at stronger torques, see the left panel of Figure 4B. This result is in good agreement with the torque-DNA occupancy fraction curves shown in the right panel of Supplementary Figure S5b that demonstrate torque-induced promotion of the DNA interaction with IHF proteins at these conditions. Furthermore, from the left panel of Figure 4B it can be seen that the shapes of the torque-extension curves in the case of IHF-covered DNA are much smoother than in the case of bare DNA, suggesting that in the former situation torque-induced decrease of the DNA extension is mainly caused by stronger DNA bending by IHF proteins rather than by formation of supercoiled structures typical for bare DNA.

At larger positive torques ($\tau \geq 15$ pN·nm), however, the torque-extension curves of DNA interacting with IHF proteins become practically identical to those obtained for bare DNA [compare the left panels of Figure 2B and Supplementary Figure S2b], indicating IHF dissociation from the DNA due to formation of supercoiled bare DNA structures. Similarly, application of strong negative torques ($\tau < -11$ pN·nm) also results in destabilization of nucleoprotein complexes formed by IHF proteins, but this time this happens due to the DNA transition into alternative L-DNA structural state, which is manifested by the increase in the DNA extension and the large drop in the DNA superhelical density.

Indeed, the right panel of Supplementary Figure S2b demonstrating the DNA superhelical density curves versus the applied torsional stress shows that at extreme negative ($\tau < -11$ pN·nm) and positive ($\tau > 35$ pN·nm) torques, where DNA experiences transitions into L- and P-DNA states, the curves look identical to those obtained in the case of bare DNA [Figure 2B, right panel]. This result suggests that similarly to DNA-stiffening proteins, IHF binding to B-DNA does not have a strong effect on the DNA transitions into alternative structural states, such as L- and P-DNA, as the protein binding energy to DNA measured per single DNA base-pair ($\mu_{pr} = 2.0\, k_B T$ / 36 bp $\approx 0.06\, k_B T$ per bp) is much smaller than the free energy associated with the DNA transitions between different structural states ($\mu_u \sim 3 - 20\, k_B T$ per base-pair, where $u =$ L or P, see Table 1).

Thus, it can be concluded that the most prominent changes in the conformation of DNA due to its interaction with DNA-bending proteins mostly take place in a narrow range of torques ($-11 \leq \tau \leq 16$ pN·nm) and only at sufficiently low forces applied to DNA ($f < 1.5$ pN). Indeed, as Supplementary Figure S5b shows, only in this range the IHF density on the DNA becomes sufficiently high to alter its spatial organization.

Finally, from the torque-superhelical density curves presented in the right panel of Figure 4B it can be seen that the superhelical density of IHF-covered DNA switches from a negative value at negative torques to a positive value at positive torques, once again demonstrating that nucleoprotein complexes formed by DNA-bending proteins can easily flip between left- and right-handed conformations depending on the sign of the applied torque.

Effects of DNA-wrapping proteins on the DNA mechanical response to force and torque constraints

The final group of architectural proteins, which we studied in this work, were DNA-wrapping proteins that not only promote formation of compact nucleoprotein complexes upon binding to DNA, but also make a well-defined fixed contribution to the total DNA linking number. In this section, we explore two famous examples of DNA-wrapping proteins: (i) histone octamers that wrap ∼147 bp of DNA into a left-handed solenoidal structures known as a nucleosomes (23,24,35), and (ii) histone $(H3\text{-}H4)_2$ tetramers that wrap ∼73 bp of DNA into tetrasomes—half nucleosome complexes that do not possess significant chiral preference, flipping between left- and right-handed conformations (99,100). Here we show how the effects of force and torque constraints applied to DNA influence on its interaction with these two protein complexes, which serve as specific examples of chiral and achiral DNA-wrapping proteins.

Since the X-ray crystal structure of nucleosomes has been previously solved (23,24), we used it as a template for constructing the model of nucleosome complexes, which is

demonstrated on schematic Figure 1F. As for tetrasomes, their exact structure is not known yet. For this reason, we modelled them simply as a half (left-handed tetrasomes) or a mirrored half (right-handed tetrasomes) of nucleosome complexes that wrap ∼73 bp of DNA (101), see Figure 1E.

Furthermore, due to the absence of experimental data regarding the elastic properties of nucleosomes and tetrasomes, the bending and twisting rigidities of the entry and exit DNA segments of these nucleoprotein complexes for simplicity were set equal to the same values as in the case of DNA-stiffening and DNA-bending proteins considered in the previous sections: $a_{pr} = c_{pr} = 33.3$, see Table 2. Although we would like to emphasize that in contrast to the case of DNA-stiffening proteins, bending and twist rigidities of the entry and exit DNA segments of DNA-wrapping proteins play less significant roles in determining the mechanical response of protein-covered DNA to force and torque constraints, assuming that the protein binding energy to DNA, μ_{pr}, is fixed at a constant value. Thus, a_{pr} and c_{pr} parameters have rather negligible impact on the results presented in this section.

In contrast, the binding energies of histone tetramers and octamers to DNA play the major roles in determining stabilities of tetrasome and nucleosome complexes under force and torque constraints applied to the DNA. While the exact values of these energies are not yet known, estimations based on single-molecule experimental data indicate that the value of the DNA-binding energy of histone octamers is likely to be of the order of $\sim 40\ k_B T$ (102).

In addition, single-DNA manipulation assays show that the energy associated with the unwrapping of the first DNA turn (known as outer nucleosome turn) from histone octamers equals to $12.0\ k_B T$ (43), and while there is no similar data for the remaining part of the nucleosome-bound DNA (inner nucleosome turn), the same experiments indicate that its affinity to histone octamers may approximately be twice as big (43,103). Hence, taken together, both outer and inner nucleosome turns add up to $\sim 40\ k_B T$ of the nucleosome protein core binding energy to DNA, in good agreement with the chromatin stretching experiments reported in ref. (102). For this reason, in all our nucleosome calculations the DNA-binding energy of histone octamers to DNA was set equal to $\mu_{pr} = 40.0\ k_B T$.

Furthermore, existing single-molecule data suggest that the inner nucleosome turn is formed by H3/H4-DNA interactions (45). Thus, the energy associated with the unwrapping of the inner nucleosome turn may be regarded as the binding energy of $(H3\text{-}H4)_2$ histone tetramers to DNA. On top of that, experimental measurements reveal that left-handed tetrasomes have $2.3\ k_B T$ energy preference over right-handed tetrasomes (100). Based on these observations the DNA-binding energies for the left- and right-handed tetrasomes were put equal to $\mu_{pr}^{left} = 26.3\ k_B T$ and $\mu_{pr}^{right} = 24.0\ k_B T$ in all of the computations presented below.

Finally, as mentioned at the beginning of this section, formation of nucleosome and tetrasome complexes on DNA is accompanied by the change in the total DNA linking number by a well-defined amount, ΔLk_{pr}, per each nucleoprotein complex. From the existing experimental data it is known that the DNA linking number change due to the DNA wrapping around the nucleosome core is $\Delta Lk_{pr} \sim -1.2$ (100,104); whereas, in the case of tetrasomes, experimentally measured DNA linking number changes associated with the left- and right-handed tetrasome conformations are equal to $\Delta Lk_{pr}^{left} = -0.73$ and $\Delta Lk_{pr}^{right} = +1.0$, respectively (100). Thus, in all of the transfer-matrix calculations, assembly of nucleosome and tetrasome complexes on DNA was associated with the respective DNA linking number changes, see Table 2.

Substituting the values of the above model parameters into Equation (F11)–(F12) in Supplementary Appendix F3 and using the resulting DNA transfer-matrices to calculate the DNA partition function, we plotted the force- and torque-extension curves $[z(f)|_{\tau=\tau_0}$ and $z(\tau)|_{f=f_0}]$ as well as the force- and torque-superhelical density curves of DNA $[\sigma(f)|_{\tau=\tau_0}$ and $\sigma(\tau)|_{f=f_0}]$ at fixed force ($f = f_0$) and torque ($\tau = \tau_0$) constraints in the presence of tetrasome and nucleosome complexes formation on DNA. The final results of the computations are shown in Figures 5 and 6; and Supplementary Figures S3 and 4.

From the left top and bottom panels of Figure 5A it can be seen that histone tetramers bind to DNA and promote its collapsing into a compact conformation in a wide range of the applied force and torque constraints. Interestingly, shift of the force-extension curves calculated for DNA interacting with histone tetramers [solid lines in Figure 5A] towards higher force values with the increasing magnitude of the applied torque suggests that torsional stress of both positive and negative sign facilitates tetrasomes formation, resulting in a more stable compaction of the DNA. This torque-induced effect can be even more clearly observed on the left and middle panels of Supplementary Figure S6a and b demonstrating the change of the average DNA occupancy fraction by tetrasome complexes as a function of the applied force and torque constraints.

One of the most prominent features that stands out in Supplementary Figure S6a and b is that both positive and negative torques promote formation of tetrasomes with correspondingly right- and left-handed complex chiralities, resulting in the respective jump of the DNA superhelical density to $\pm(0.06-0.13)$, where the sign of the change is determined by the chirality of the formed nucleoprotein complexes [see the right panels of Figure 5A]. These results are in good agreement with the previously published experimental data (100), suggesting that transfer-matrix calculations correctly reproduce behaviour of tetrasome complexes revealed in single-molecule experiments.

Furthermore, from Supplementary Figure S6a and b it can be seen that whilst being stable at low and moderate tensions ($f < 5 - 9$ pN), tetrasomes quickly become destabilized by forces $f > 6 - 10$ pN, resulting in complete dissociation of histone tetramers from DNA. Thus, it can be concluded that tetrasomes respond to the force and torque constraints in a completely opposite way than DNA-stiffening proteins—whilst the latter prefer torsionally relaxed DNA stretched by a mechanical force, tetrasomes mostly bind to twisted DNA being under sufficiently low tension.

Such a distinct behaviour of the two types of DNA-binding proteins stems from the large difference in the geo-

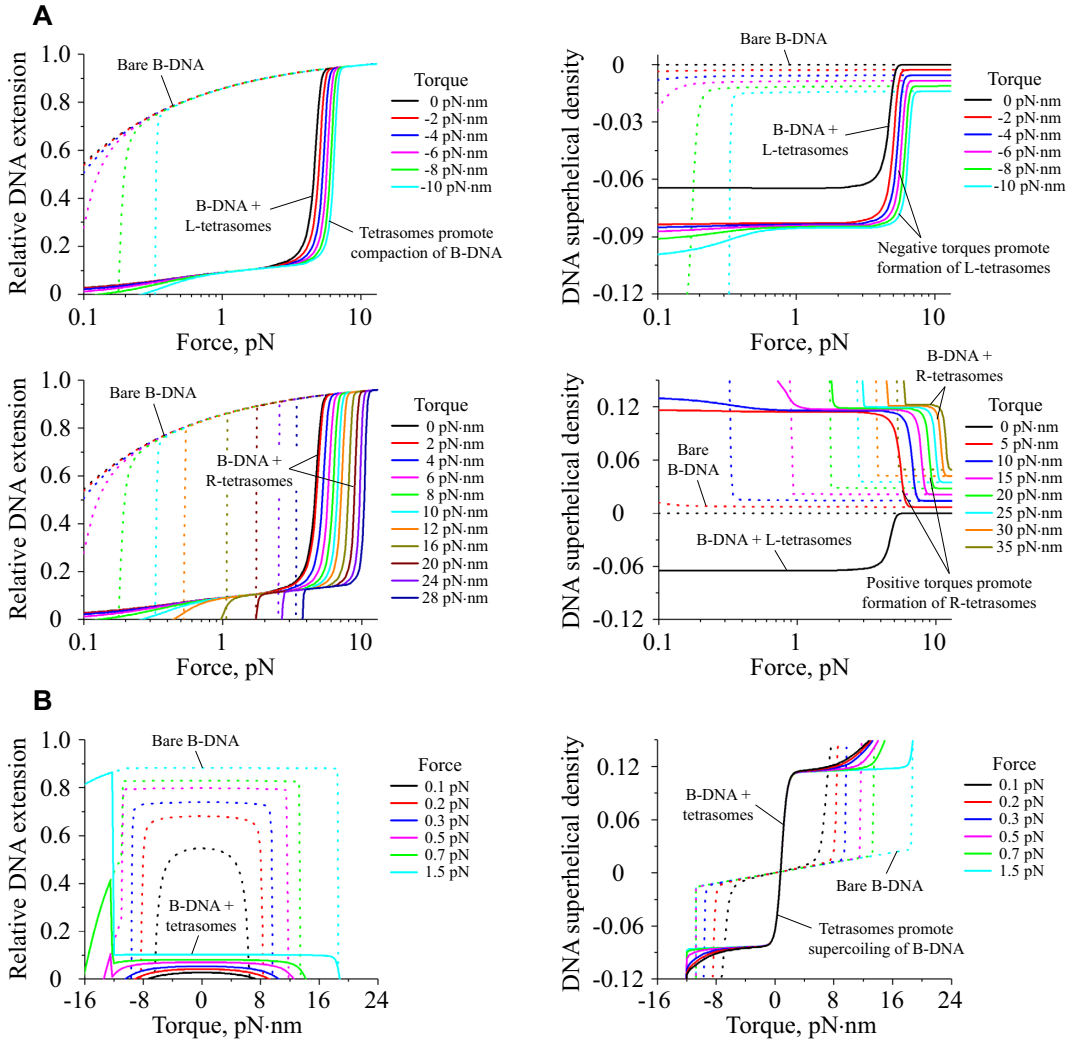

Figure 5. Mechanical response of DNA to the applied force and torque constraints in the presence of DNA interactions with histone tetramers. The figure shows (**A**) force-extension and force-superhelical density curves obtained at different values of the torque, τ, as well as (**B**) torque-extension and torque-superhelical density curves obtained at different values of the force, f, exerted to the DNA. Solid curves demonstrate the behaviour of DNA in the presence of histone tetramers; whereas, dotted curves indicate mechanical response of bare DNA under the same force and torque constraints. As can be seen from the top and bottom plots on panel (A), formation of tetrasome complexes on DNA leads to the molecule collapsing into a compact conformation, which is accompanied by the change in the DNA superhelical density, whose sign depends on the magnitude and direction of the applied torque. While tetrasomes can easily switch between the left- and right-handed structures, their slight preference to assume the left-handed conformation results in somewhat asymmetric behaviour of the DNA force-superhelical density curves with respect to positive and negative torques, as can be seen from the right graphs of panel (A). Nevertheless, torque-extension and torque-superhelical density curves displayed on panel (B) still demonstrate rather symmetric shapes up to the point when DNA experiences transition into alternative L-DNA state at $\tau \sim -11$ pN·nm torque. In all panels, the DNA extension is normalized to the total contour length of DNA in B-form. Abbreviations L-tetrasomes and R-tetrasomes are used to indicate left- and right-handed tetrasome complexes, respectively.

metric and topological characteristics of their nucleoprotein complexes. Namely, DNA wrapping by histone tetramers results in −0.73/+1.0 DNA linking number change, which leads to a strong stabilization effect of the left- and right-handed tetrasomes at high torques of the corresponding sign caused by the significant decrease of the terasomes' torque-dependent potential energy. On the other hand, DNA-stiffening proteins predominantly form straight rigid nucleoprotein filaments on DNA that rather easily lose their stability when either positive or negative torque is applied to the DNA, see the DNA-stiffening protein section.

Furthermore, DNA compaction by tetrasomes results in a situation when mechanical stretching of DNA works against formation of tetrasome complexes, which eventually leads to destabilization of tetrasomes by the applied force. In contrast, sufficiently strong tension exerted on DNA promotes its interaction with DNA-stiffening proteins due to purely entropic reasons discussed in the DNA-stiffening protein section.

Finally, it should be noted that besides having different response to force and torque constraints, tetrasomes and DNA-stiffening complexes also have very distinct effects on the global DNA conformation, which are not only can

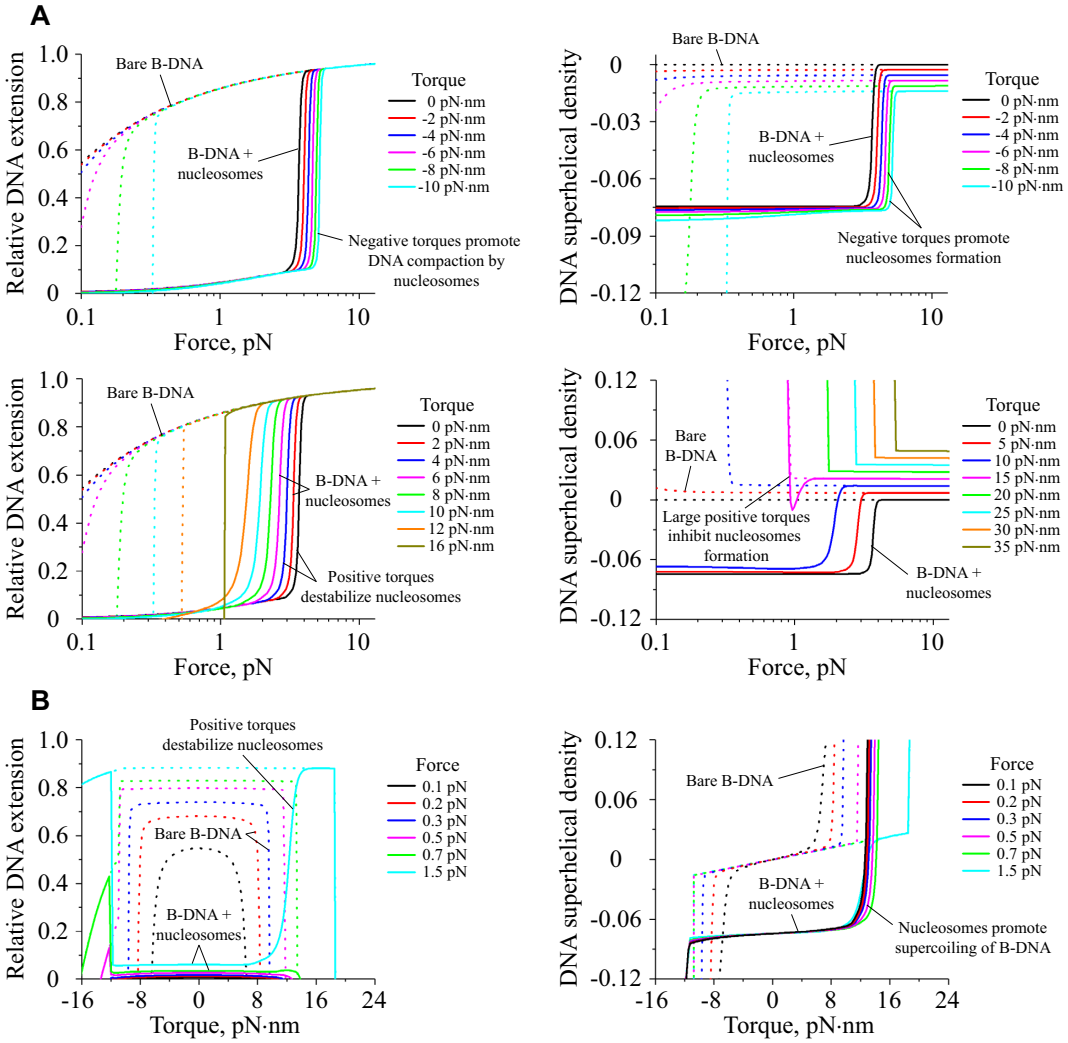

Figure 6. Mechanical response of DNA to the applied force and torque constraints in the presence of DNA interactions with histone octamers. The figure shows (**A**) force-extension and force-superhelical density curves obtained at different values of the torque, τ, as well as (**B**) torque-extension and torque-superhelical density curves obtained at different values of the force, f, exerted to the DNA. Solid curves demonstrate the behaviour of DNA in the presence of histone octamers that upon binding to DNA form nucleosome complexes; whereas, dotted curves indicate mechanical response of bare DNA under the same force and torque constraints. In contrast to histone tetrasomes, nucleosomes always assume the left-handed conformation and, as a result, form on DNA only at negative ($\tau < 0$ pN·nm) or moderate positive torques ($0 < \tau < 15$ pN·nm). Indeed, it can be seen from panels (A) and (B) that upon binding to DNA, histone octamers collapse it into a compact conformation in $-11 \leq \tau < 15$ pN·nm torque range; whereas, application of a higher positive torsional stress to DNA ($\tau \geq 15$ pN·nm) leads to destabilization of nucleosome complexes, which eventually give a way to formation of supercoiled bare DNA structures. As for large negative torques ($\tau < -11$ pN·nm), under these conditions DNA experiences transition into alternative L-DNA form, which drives dissociation of histone octamers from the DNA. In all panels, the DNA extension is normalized to the total contour length of DNA in B-form.

be clearly seen from the DNA force-extension and force-superhelical density curves shown in Figures 3A and 5A, but also strongly pronounced in the behaviour of the DNA torque-extension and torque-superhelical density curves presented in Figures 3B and 5B. Indeed, direct comparison between the left panels of Figures 3B and 5B demonstrates that whilst DNA interaction with DNA-stiffening proteins results in widening of the DNA torque-extension curves in the force range of $0 \leq f \leq 3$ pN due to formation of rigid nucleoprotein filaments delaying the DNA buckling transition into a supercoiled conformation, binding of histone tetramers to DNA leads to almost complete collapsing of the torque-extension curves as a result of assembly of compact tetrasome complexes on the DNA.

It is also interesting to note from the right panels of Figures 4B and 5B that whilst nucleoprotein complexes formed by DNA-bending proteins and histone tetramers both can easily flip between the left- and right-handed conformations, the DNA torque-superhelical density curves corresponding to these complexes exhibit very different behaviours. In the case of tetrasomes, these curves reach two plateaus: ~ -0.09 at negative torques ($-10 \leq \tau < 0$ pN·nm) and ~ 0.12 at positive torques ($0 < \tau \leq 30$ pN·nm) applied to the DNA, see the right panels of Figure 5B and Supplementary Figure S3b; whereas, in the case of DNA-bending protein, IHF, no such plateaus can be observed, see the right panels of Figure 4B and Supplementary Figure S2b. The main reason for such distinct behaviour of the two

proteins is previously mentioned fact that histone tetramers make a well-defined contribution to the DNA linking number change upon formation of tetrasome complexes on the DNA. At the same time, the contribution of DNA-bending proteins, such as IHF, to the DNA linking number mainly depends on the relative orientations of the resulting nucleoprotein complexes with the respect to the rest of the DNA, which can be changed by modulating the magnitude and sign of the torque applied to the DNA.

As for nucleosomes, their behaviour is practically identical to that of left-handed tetrasomes. Namely, from the top left panel of Figure 6A it can be seen that nucleosomes promote collapsing of DNA into a compact conformation with the resulting effect being enhanced by negative torques applied to DNA. Indeed, the left panel of Supplementary Figure S6c shows that larger negative torques facilitate formation of nucleosome complexes on DNA. On the other hand, the bottom left panel of Figure 6A and the middle panel of Supplementary Figure S6c indicate that application of large positive torques to DNA results in strong destabilization of nucleosomes, causing DNA unwrapping from histone octamers with their subsequent dissociation from the DNA.

Such asymmetric response of nucleosome complexes to the applied torque constraints can be also clearly seen in the left panel of Figure 6B demonstrating the DNA torque-extension curves in the presence of DNA interaction with histone octamers (solid lines). The figure shows that whilst DNA is compacted by nucleosome complexes in the torque range of $-11 \leq \tau \leq 15$ pN·nm, at large positive torques ($\tau > 15$ pN·nm) it behaves in the same way as in the absence of histone octamers in solution, suggesting that histone octamers dissociate from DNA at these conditions [for more details compare the left panels of Figure 2B and Supplementary Figure S4b].

The above observations result from the fact that due to the negative linking number change of DNA upon formation of nucleosome complexes ($\Delta Lk_{pr} = -1.2$), negative torsional stresses applied to the DNA decrease the torque-dependent potential energy of nucleosome complexes, enhancing their stability and promoting their formation on DNA; whereas, positive torques result in the nucleosomes' potential energy increase, which eventually drives dissociation of histone octamers from DNA.

Furthermore, from the right panels of Figure 6 that show the force- and torque-superhelical density curves of DNA interacting with histone octamers it can be seen that inability of nucleosome complexes to change their chirality by flipping from the left-handed to a right-handed conformation results in the negative superhelical density of DNA (~ -0.08), which is covered by nucleosome complexes. In addition, this leads to appearance of only one, negative plateau (~ -0.08), in torque-superhelical density curves at $-11 \leq \tau \leq 15$ pN·nm torques, in sharp contrast to the the case of tetrasome complexes, whose capability to switch between the left- and right-handed conformations causes formation of the two plateaus (negative and positive) in the torque-superhelical density curves, see the right panel of Figure 5B.

Force-torque phase diagrams of DNA structures and DNA–protein complexes

Using the obtained theoretical results, we have plotted force-torque phase diagrams that show the transition boundaries between different structural states of DNA and/or DNA–protein complexes for the five scenarios considered in the above sections, including the bare DNA case and DNA interacting with the four different types of DNA-architectural proteins, see Figure 7.

The boundaries between B- and L-DNA as well as between B- and P-DNA structural states were defined as the set of points (f, τ) at which ∼50% of the DNA segments are in L- or P-DNA forms, respectively. Furthermore, the boundary between extended and supercoiled conformations of DNA in a particular structural state was determined as a set of points at which DNA extension experiences ∼50% drop with respect to the value predicted by the worm-like chain model for the corresponding form of DNA being in a torsionally relaxed state.

Finally, the boundaries between bare DNA and protein-covered DNA states were assumed to pass through the points at which half of the maximum DNA-binding sites are occupied by the studied protein. Here we would like to note that the total number of DNA-binding sites is not necessarily equivalent to the total number of DNA segments, see, for example, Supplementary Figure S6c showing that the maximum occupancy fraction of DNA by nucleosomes never goes above ∼90%. The main reason for this is the existence of bare DNA gaps between nucleoprotein complexes that correspond to DNA linkers connecting neighbouring protein–DNA complexes. In the case of reconstituted nucleosome arrays or densely packed yeast chromatin, the minimal length of such DNA linkers was found to be of the order of $\sim 10 - 20$ bp (105,106). For this reason, the minimal possible spacing between neighbouring nucleosomes was set to 18 bp (i.e. 12 DNA segments) in all of the transfer-matrix calculations. The same minimal length of the DNA linkers was also used in the computations of DNA interacting with histone tetramers and IHF proteins, as previously reported structural data suggest that such linkers likely exist in-between nucleoprotein complexes formed by IHF proteins as well (22), see Supplementary Appendices F2–F3 for details.

The resulting phase diagrams plotted using the above definitions for the DNA transition boundaries for the cases of bare DNA and DNA interacting with DNA-stiffening, DNA-bending (IHF) and DNA-wrapping proteins (hitone tetramers and octamers) are depicted on Figure 7.

Whilst the case of bare DNA has been previously discussed in details in our earlier publications (75,76), here we will mainly focus on the description of the rest of the phase diagrams using the bare DNA graph shown in Figure 7A as a reference point to identify main changes in the DNA behaviour upon addition of different DNA-binding proteins into solution.

The next panel, [Figure 7B], demonstrates the phase diagram of DNA in the presence of nucleoprotein filaments formation by DNA-stiffening proteins. As can be seen from the figure, proteins binding to DNA leads to the leftward and rightward shifts of the boundaries between extended

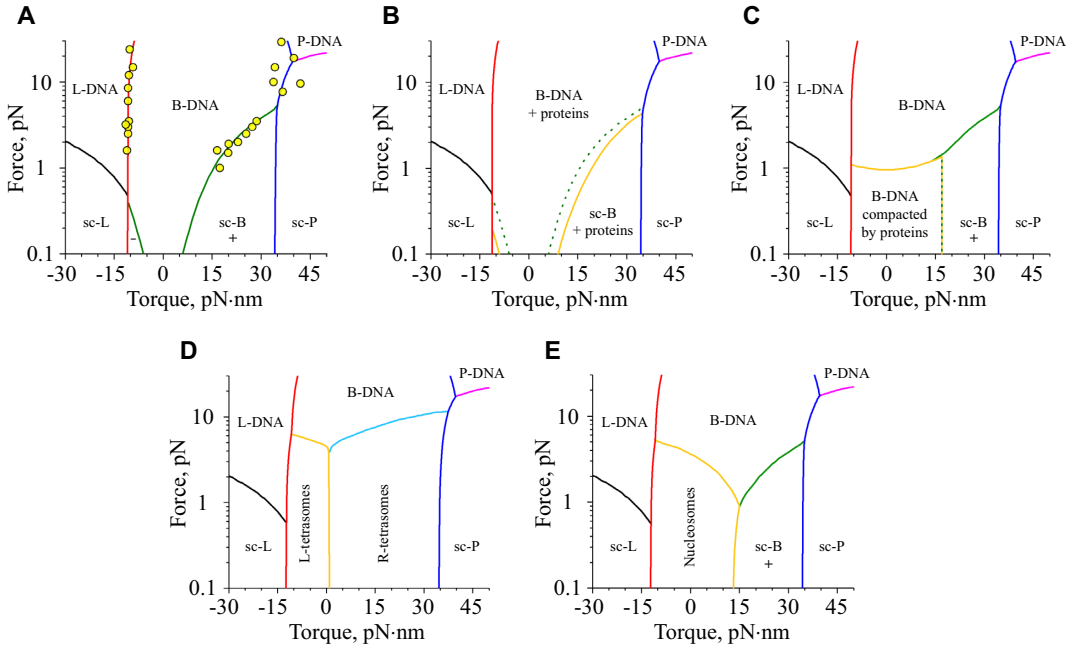

Figure 7. DNA phase diagrams. The figure shows force-torque phase diagrams for: bare DNA (**A**), DNA interacting with DNA-stiffening (**B**) and DNA-bending proteins (**C**) as well as for DNA in the presence of tetrasome (**D**) and nucleosome (**E**) complexes formation. Solid curves predicted by the transfer-matrix calculations indicate transition boundaries between extended (B, L and P) and supercoiled (sc-B, sc-L and sc-P) states of DNA as well as between various DNA–protein conformations. Presented phase diagrams summarize all of the theoretical results plotted in Figures 2-6. From the figure, it can be seen that while DNA-stiffening proteins delay formation of supercoiled DNA structures, forcing DNA to stay in the extended conformation (i.e. the boundary in panel (B) between B-DNA and sc-B states recedes to higher values of the applied torque), DNA-bending and wrapping proteins promote DNA compaction via assembly of nucleoprotein complexes inducing DNA supercoiling. Circles in the phase diagram of bare DNA (A) indicate experimental data points, which were digitized from ref. (56,58,77,79–81,93). Dotted lines in panel (B) demonstrate position of the boundary between extended and supercoiled B-DNA states in the absence of DNA-stiffening proteins in solution (i.e. in the case of bare DNA).

and supercoiled B-DNA conformations at negative and positive torques, respectively, comparing to the case of bare DNA. Such receding of the DNA supercoiling transition boundaries results from the delay in the DNA buckling transition due to the DNA-stiffening effect produced by rigid nucleoprotein filaments, which polymerize on DNA upon proteins binding to it, see the DNA-stiffening protein section for more details.

In the case of DNA interaction with the DNA-bending protein (IHF), the most prominent effect that can be seen from the phase diagram displayed on Figure 7C is appearance of a new DNA–protein state in $-11 \leq \tau \leq 17$ pN·nm torque range and at forces $f < 1.0 - 1.5$ pN that corresponds to the formation of compact nucleoprotein complexes by IHF proteins on DNA. As the transfer matrix calculations show, these complexes assume left-handed chirality at negative torques ($-11 \leq \tau < 0$ pN·nm) and, more importantly, have free energy, which is smaller than the energy of supercoiled bare B-DNA, see the DNA-bending protein section for more details. This results in complete disappearance of the latter state from the phase diagram of IHF-bound DNA at negative torques. At positive torques, however, the DNA behaviour is slightly more complicated. While at $0 < \tau \leq 17$ pN·nm torques IHF binding to DNA leads to formation of compact nucleoprotein complexes with right-handed chirality, further increase of the torque causes dissociation of IHF proteins from DNA, which give a way to formation of positively supercoiled bare B-DNA structures.

The final two panels shown in Figure 7D and E demonstrate the phase diagrams of DNA in the presence of tetrasome (D) and nucleosome (E) complexes formation. From Figure 7D it can be seen that in the case of tetrasomes, the most prominent changes emerging on the phase diagram of DNA is appearance of the two new DNA states corresponding to assembly of the left-handed tetrasomes at negative torques and right-handed tetrasomes at positive torques. Interestingly, in contrast to DNA-bending proteins, strong drop in the DNA free energy associated with the formation of tetrasome complexes not only leads to complete disappearance of the supercoiled bare B-DNA state at negative torques, but at positive torques as well.

In the case of nucleosomes, Figure 7E demonstrates that they form in a more narrow torque range ($-11 \leq \tau \leq 15$ pN·nm) comparing to tetrasome complexes. Indeed, as the transfer-matrix calculations discussed in the DNA-wrapping protein section show, nucleosomes become highly destabilized at large positive torques due to their left-handed chirality. As a result, while nucleosomes assembly on DNA leads to disappearance of supercoiled bare B-DNA state at negative torques, at high positive torques ($\tau \geq 15$ pN·nm) DNA keeps developing supercoiled structures that drive dissociation of histone octamers from the DNA. Another interesting feature that can be seen in Figure 7E is a rather steep boundary between the nucleosome-covered and extended bare B-DNA states, indicating that nucleosomes formation on B-DNA is more sensitive to the ap-

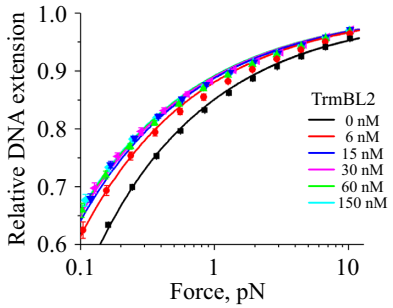

Figure 8. Force-extension curves of DNA in the presence of different amounts of TrmBL2 protein in solution. The figure shows fitting of the experimentally measured force-extension curves of DNA obtained at different concentrations of DNA-stiffening protein, TrmBL2, in solution to the theoretical results predicted by the transfer-matrix theory. Solid symbols on the plot represent the experimental data points collected during stretching cycles of λ-DNA; whereas, solid curves demonstrate theoretical data fitting based on the transfer-matrix calculations described in the main text. Error bars show experimental SEM values of the corresponding data points.

plied torque constraints than in the case of other nucleoprotein complexes discussed in this work—an effect which may be employed by living cells in regulation of the chromatin structure and its spatial organization.

Application of the transfer-matrix theory for processing of experimental data

To demonstrate practical utility of the transfer-matrix formalism, in this section we describe how to exploit it in order to extract valuable information about DNA–protein interactions from experimentally measured force-extension curves of DNA. For this purpose, we use experimental data obtained on a torsionally relaxed 48 502 bp λ-DNA incubated in the presence of different amounts of TrmBL2 protein in solution (33).

It has been shown in our previous study that TrmBL2 is a DNA-stiffening protein, which binds to DNA in a cooperative manner, resulting in polymerization of rigid nucleoprotein filaments (33). Furthermore, it has been found that TrmBL2 has two different binding modes to DNA, which manifest themselves in a protein concentration-dependent manner (33). Whilst it is not hard to introduce both of these modes into the transfer-matrix calculations [see comments at the end of the '*General Theory*' section], here we deal only with the experimental data obtained at $0 - 150$ nM protein concentrations, at which TrmBL2 interaction with DNA can be described by a single binding mode (33). This makes it possible to directly use Supplementary Equation (F6) and (6) in order to fit experimentally measured force-extension curves of DNA (solid symbols in Figure 8) in the presence of TrmBL2 protein in solution to the theoretical graphs predicted by the transfer-matrix theory (solid lines in Figure 8).

For the fitting procedure we used the Nelder–Mead simplex algorithm (107), which enables to search for the optimal values of the model parameters at which the total deviation between the experimental data points and the theoretical curves is minimal. To fit the data, the following three model parameters were varied in the calculations: (i) the bending persistence length of protein-covered DNA [A_{pr}], (ii) equilibrium dissociation constant of the protein from DNA [K_d] and (iii) the cooperative binding energy of proteins to DNA [J_{pr}]. At each algorithm step, the proteins' binding energy to DNA at a given concentration, c, of TrmBL2 in solution was calculated using the following classical formula: $\mu_{pr} = \ln(c/K_d)$. The final results in the form of DNA force-extension curves predicted by the transfer-matrix theory for the optimum values of the model parameters are shown in Figure 8.

As can be seen from the figure, the theoretical graphs demonstrate very good agreement with the experimental data. Furthermore, the obtained optimal values of the model parameters: $A_{pr} = 88$ nm, $K_d = 3.8$ nM and $J_{pr} = 4.26\ k_BT$ are very close to those previously reported in ref. (33), which were acquired by an independent method via fitting the experimental data to the Marko–Siggia formula and Hill equation. This consistency indicates that the transfer-matrix theory presented in this study accurately describes DNA–protein interactions and can be easily implemented for extraction of important information regarding the DNA-binding affinities of studied proteins and physical properties of nucleoprotein complexes from single-molecule experiments performed on individual DNA molecules.

DISCUSSION

In this study, we have developed a new theoretical approach based on the transfer-matrix calculations for investigation of DNA–protein interactions under force and torque constraints, which makes it possible to evaluate changes in the DNA conformation due to formation of nucleoprotein complexes by DNA-binding proteins in a wide range of mechanical forces applied to the DNA. As a result, the constructed theoretical framework may be used in future to provide better understanding of the potential role of such constraints in regulation of the DNA-binding properties of different types of DNA-architectural proteins.

It should be noted that although in this study the transfer-matrix approach has been demonstrated using examples of proteins which equally well bind to all of the DNA segments, the nature of the transfer-matrix formalism easily allows one to include sequence-dependent behaviour of DNA-binding proteins into the calculations. Indeed, according to Equation (6), the DNA partition function is determined by the product of transfer matrices, which are defined locally on the vertices connecting neighbouring DNA segments in the polygonal chain representing the DNA polymer. Thus, proteins sequence-specific binding to DNA can be straightforwardly implemented by introduction of site-dependent DNA transfer-matrices, $\mathbf{L}_j$ ($j = 1, ..., N-1$), and replacement of $\mathbf{L}^{N-1}$ matrices product with $\prod_{j=1}^{N-1} \mathbf{L}_j$ in Equation (6).

Furthermore, flexibility of the developed transfer-matrix approach makes it possible not only use it to study formation of nucleoprotein complexes by a single type of DNA-architectural proteins at a time, but, more importantly, to investigate competitive binding of different types of proteins to the same DNA and its potential regulation by mechanical constraints applied to the DNA. Indeed, calculations

presented in this study demonstrate that force and torque constraints imposed on DNA frequently have a strong effect on the proteins' DNA-binding affinity, whose strength may either increase or drop depending on the architecture of the nucleoprotein complexes as well as the magnitude and direction of the applied mechanical forces. These results immediately imply that by changing the mechanical constraints it may be possible to modulate the balance between nucleoprotein complexes formed on DNA by different groups of DNA-binding proteins, warranting future study.

Considering mounting experimental evidences showing that the chromosomal DNA in living cells is subject to a large number of various mechanical constraints, and taking into account that there exist many different types of DNA-binding proteins involved in regulation of the DNA organization inside living cells, this kind of research may help to gain better understanding of how the force- and torque-dependent interaction of DNA-architectural proteins and transcription factors with DNA results in experimentally observed activation or suppression of a number of specific genes in response to mechanical forces applied to the nucleus and/or chromosomal DNA in living cells (17,18,19,20,21).

Finally, it should be noted that the transfer-matrix calculations developed in this study appear to be much faster than the existing Brownian/molecular dynamics simulation (MD) and Metropolis-Monte Carlo (MC) computation algorithms, which are frequently used to model DNA behaviour under mechanical constraints in the presence or absence of DNA-binding proteins (62,63,65–68,70,71). For example, computation of torque-extension curves of a micrometer size DNA could be done in several seconds by running transfer-matrix calculations on a laptop, while for MC algorithm it takes several days of intensive calculations on a computer cluster to obtain similar results (data not shown). This gives the transfer-matrix approach a strong advantage in interpretation of experimental data obtained in single-DNA manipulation assays.

Indeed, as demonstrated in the example of DNA interaction with TrmBL2 proteins at the end of the *'Results'* section, fast transfer-matrix calculations described in our study allow one to vary parameters to achieve best fitting to the experimentally measured force- and torque-extension curves as well as force- and torque-superhelical density curves of DNA in a sufficiently short amount of time. By doing so, it is possible to obtain accurate and detailed information about the DNA-binding affinities of studied proteins and physical properties of nucleoprotein complexes formed on DNA from the experimental data, providing important information about the role of force and torque constraints in regulation of DNA–protein interactions.

For this reason, we believe that the transfer-matrix formalism presented in our work may be used in future to quickly estimate potential changes in the DNA conformation under various mechanical constraints imposed on DNA in the presence or absence of DNA-binding proteins in surrounding environment, pinpointing the most important questions and problems that can be later studied in detail by utilizing the classical MD and MC simulation methods. By utilizing such a combination of the transfer-matrix calculations and MD/MC algorithms, it will be then possible to gain deep insights into the role of force and torque constraints in modulation of DNA–protein interactions, which will be important for better understanding of multiple experimental findings suggesting a major role of mechanical forces in regulation of the cell genome organization.

In summary, the transfer-matrix formalism developed in this study allows one to gain valuable insights into physical processes governing formation of nucleoprotein complexes by DNA-binding proteins under force and torque constraints applied to the DNA. The flexibility and advantages of this method make it a powerful tool for a broad range of future applications, including but not limited to investigation of the DNA organization by multiple DNA-binding proteins as well as processing and interpretation of single-molecule experimental data obtained in single-DNA manipulation assays.

SUPPLEMENTARY DATA

Supplementary Data are available at NAR Online.

ACKNOWLEDGEMENTS

We would like to thank Irina Belyanskaya, Ladislav Hovan and Yang Kaiyuan for their invaluable help in translation of the transfer-matrix calculation programs into C++ language and uploading of the program source files to the internet.

FUNDING

Ministry of Education (Singapore) Academic Research Fund Tier 3 [MOE2012-T3-1-001]; National Research Foundation (NRF); Prime Minister's Office, Singapore under its NRF Investigatorship Programme (NRF Investigatorship) [NRF-NRFI2016-03]; National Research Foundation (Singapore) through the Mechanobiology Institute Singapore (to J.Y.). Funding for open access charge: National Research Foundation (Singapore) through the Mechanobiology Institute Singapore.
Conflict of interest statement. None declared.

REFERENCES

1. Luijsterburg,M.S., White,M.F., van Driel,R. and Dame,R.T. (2008) The major architects of chromatin: architectural proteins in bacteria, archaea and eukaryotes. *Crit. Rev. Biochem. Mol. Biol.*, **43**, 393–418.
2. Dame,R.T. and Dorman,C.J. (2010). *Bacterial Chromatin*. Springer, Heidelberg.
3. Bannister,A.J. and Kouzarides,T. (2011) Regulation of chromatin by histone modifications. *Cell Res.*, **21**, 381–395.
4. Champoux,J.J. (2001) DNA topoisomerases: structure, function, and mechanism. *Annu. Rev. Biochem.*, **70**, 369–413.
5. Hübscher,U., Maga,G. and Spadari,S. (2002) Eukaryotic DNA polymerases. *Annu. Rev. Biochem.*, **71**, 133–163.
6. Rothwell,P.J. and Waksman,G. (2005) Structure and mechanism of DNA polymerases. *Adv. Protein Chem.*, **71**, 401–440.
7. Singleton,M.R., Dillingham,M.S. and Wigley,D.B. (2007) Structure and mechanism of helicases and nucleic acid translocases. *Annu. Rev. Biochem.*, **76**, 23–50.
8. Buc,H. and Strick,T. (2009). *RNA Polymerases as Molecular Motors*. RSC Publishing, Cambridge.

9. Spies,M. (2013). *DNA Helicases and DNA Motor Proteins*. Springer, NY.
10. Wang,M.D., Schnitzer,M.J., Yin,H., Landick,R., Gelles,J. and Block,S.M. (1998) Force and velocity measured for single molecules of RNA polymerase. *Science*, **282**, 902–907.
11. Strick,T.R., Croquette,V. and Bensimon,D. (2000) Single-molecule analysis of DNA uncoiling by a type II topoisomerase. *Nature*, **404**, 901–904.
12. Wuite,G.J. L., Smith,S.B., Young,M., Keller,D. and Bustamante,C. (2000) Single-molecule studies of the effect of template tension on T7 DNA polymerase activity. *Nature*, **404**, 103–106.
13. Gore,J., Bryant,Z., Stone,M.D., Nöllmann,M., Cozzarelli,N.R. and Bustamante,C. (2006) Mechanochemical analysis of DNA gyrase using rotor bead tracking. *Nature*, **439**, 100–104.
14. Johnson,D.S., Bai,L., Smith,B.Y., Patel,S.S. and Wang,M.D. (2007) Single-molecule studies reveal dynamics of DNA unwinding by the ring-shaped T7 helicase. *Cell*, **129**, 1299–1309.
15. Ma,J., Bai,L. and Wang,M.D. (2013) Transcription under torsion. *Science*, **340**, 1580–1583.
16. Wang,N., Tytell,J.D. and Ingber,D.E. (2009) Mechanotransduction at a distance: mechanically coupling the extracellular matrix with the nucleus. *Nat. Rev. Mol. Cell Biol.*, **10**, 75–82.
17. Shivashankar,G.V. (2011) Mechanosignaling to the cell nucleus and gene regulation. *Annu. Rev. Biophys.*, **40**, 361–378.
18. Uhler,C. and Shivashankar,G.V. (2017) Regulation of genome organization and gene expression by nuclear mechanotransduction. *Nat. Rev. Mol. Cell Biol.*, **18**, 717–727.
19. Iyer,K.V., Pulford,S., Mogilner,A. and Shivashankar,G.V. (2012) Mechanical activation of cells induces chromatin remodeling preceding MKL nuclear transport. *Bipohys. J.*, **103**, 1416–1428.
20. Mammoto,A., Mammoto,T. and Ingber,D.E. (2012) Mechanosensitive mechanisms in transcriptional regulation. *J. Cell Sci.*, **125**, 3061–3073.
21. Tajik,A., Zhang,Y., Wei,F., Sun,J., Jia,Q., Zhou,W., Singh,R., Khanna,N., Belmont,A.S. and Wang,N. (2016) Transcription upregulation via force-induced direct stretching of chromatin. *Nat. Mater.*, **15**, 1287–1296.
22. Rice,P.A., Yang,S.-w., Mizuuchi,K. and Nash,H.A. (1996) Crystal structure of an IHF-DNA complex: a protein-induced DNA U-turn. *Cell*, **87**, 1295–1306.
23. Luger,K., Mäder,A.W., Richmond,R.K., Sargent,D.F. and Richmond,T.J. (1997) Crystal structure of the nucleosome core particle at 2.8Å resolution. *Nature*, **389**, 251–260.
24. Harp,J.M., Hanson,B.L., Timm,D.E. and Bunick,G.J. (2000) Asymmetries in the nucleosome core particle at 2.5Å resolution. *Acta Crystallogr. D Biol. Crystallogr.*, **D56**, 1513–1534.
25. Swinger,K.K., Lemberg,K.M., Zhang,Y. and Rice,P.A. (2003) Flexible DNA bending in HU-DNA cocrystal structures. *EMBO J.*, **22**, 3749–3760.
26. Skoko,D., Wong,B., Johnson,R.C. and Marko,J.F. (2004) Micromechanical analysis of the binding of DNA-bending proteins HMGB1, NHP6A, and HU reveals their ability to form highly stable DNA-protein complexes. *Biochemistry*, **43**, 13867–13874.
27. van Noort,J., Verbrugge,S., Goosen,N., Dekker,C. and Dame,R.T. (2004) Dual architectural roles of HU: formation of flexible hinges and rigid filaments. *Proc. Natl. Acad. Sci. U.S.A.*, **101**, 6969–6974.
28. Swinger,K.K. and Rice,P.A. (2004) IHF and HU: flexible architects of bent DNA. *Curr. Opin. Struct. Biol.*, **14**, 28–35.
29. Liu,Y., Chen,H., Kenney,L.J. and Yan,J. (2010) A divalent switch drives H-NS/DNA-binding conformations between stiffening and bridging modes. *Genes Dev.*, **24**, 339–344.
30. Stella,S., Cascio,D. and Johnson,R.C. (2010) The shape of the DNA minor groove directs binding by the DNA-bending protein Fis. *Genes Dev.*, **24**, 814–826.
31. Laurens,N., Driessen,R.P.C., Heller,I., Vorselen,D., Noom,M.C., Hol,F.J.H., White,M.F., Dame,R.T. and Wuite,G.J.L. (2012) Alba shapes the archaeal genome using a delicate balance of bridging and stiffening the DNA. *Nat. Commun.*, **3**, 1328.
32. Le,S., Chen,H., Cong,P., Lin,J., Dröge,P. and Yan,J. (2013) Mechanosensing of DNA bending in a single specific protein-DNA complex. *Sci. Rep.*, **3**, 3508.
33. Efremov,A.K., Qu,Y., Maruyama,H., Lim,C.J., Takeyasu,K. and Yan,J. (2015) Transcriptional repressor TrmBL2 from *Thermococcus kodakarensis* forms filamentous nucleoprotein structures and competes with histones for DNA binding in a salt- and DNA supercoiling-dependent manner. *J. Biol. Chem.*, **290**, 15770–15784.
34. Ahmad,M.U. D., Waege,I., Hausner,W., Thomm,M., Boos,W., Diederichs,K. and Welte,W. (2015) Structural insights into nonspecific binding of DNA by TrmBL2, an archaeal chromatin protein. *J. Mol. Biol.*, **427**, 3216–3229.
35. Talbert,P.B. and Henikoff,S. (2010) Histone variants – ancient wrap artists of the epigenome. *Nat. Rev. Mol. Cell Biol.*, **11**, 264–275.
36. Xiao,B., Johnson,R.C. and Marko,J.F. (2010) Modulation of HU-DNA interactions by salt concentration and applied force. *Nucleic Acids Res.*, **38**, 6176–6185.
37. Dame,R.T., Wyman,C. and Goosen,N. (2000) H-NS mediated compaction of DNA visualised by atomic force microscopy. *Nucleic Acids Res.*, **28**, 3504–3510.
38. Zhao,X., Peter,S., Dröge,P. and Yan,J. (2017) Oncofetal HMGA2 effectively curbs unconstrained (+) and (–) DNA supercoiling. *Sci. Rep.*, **7**, 8440.
39. Yan,Y., Ding,Y., Leng,F., Dunlap,D. and Finzi,L. (2018) Protein-mediated loops in supercoiled DNA create large topological domains. *Nucleic Acids Res.*, **46**, 4417–4424.
40. Jelinska,C., Conroy,M.J., Craven,C.J., Hounslow,A.M., Bullough,P.A., Waltho,J.P., Taylor,G.L. and White,M.F. (2005) Obligate heterodimerization of the archaeal Alba2 protein with Alba1 provides a mechanism for control of DNA packaging. *Structure*, **13**, 963–971.
41. Brower-Toland,B.D., Smith,C.L., Yeh,R.C., Lis,J.T., Peterson,C.L. and Wang,M.D. (2002) Mechanical disruption of individual nucleosomes reveals a reversible multistage release of DNA. *Proc. Natl. Acad. Sci. U.S.A.*, **99**, 1960–1965.
42. Yan,J. and Marko,J.F. (2003) Effects of DNA-distorting proteins on DNA elastic response. *Phys. Rev. E*, **68**, 011905.
43. Mihardja,S., Spakowitz,A.J., Zhang,Y. and Bustamante,C. (2006) Effect of force on mononucleosomal dynamics. *Proc. Natl. Acad. Sci. U.S.A.*, **103**, 15871–15876.
44. Meng,H., Andresen,K. and van Noort,J. (2015) Quantitative analysis of single-molecule force spectroscopy on folded chromatin fibers. *Nucleic Acids Res.*, **43**, 3578–3590.
45. Sheinin,M.Y., Li,M., Soltani,M., Luger,K. and Wang,M.D. (2013) Torque modulates nucleosome stability and facilitates H2A/H2B dimer loss. *Nat. Commun.*, **4**, 2579.
46. Pfaffle,P. and Jackson,V. (1990) Studies on rates of nucleosome formation with DNA under stress. *J. Biol. Chem.*, **265**, 16821–16829.
47. Garinther,W.I. and Schultz,M.C. (1997) Topoisomerase function during replication-independent chromatin assembly in yeast. *Mol. Cell. Biol.*, **17**, 3520–3526.
48. Salceda,J., Fernández,X. and Roca,J. (2006) Topoisomerase II, not topoisomerase I, is the proficient relaxase of nucleosomal DNA. *EMBO J.*, **25**, 2575–2583.
49. Shindo,H., Furubayashi,A., Shimizu,M., Miyake,M. and Imamoto,F. (1992) Preferential binding of *E. coli* histone-like protein HUα to negatively supercoiled DNA. *Nucleic Acids Res.*, **20**, 1553–1558.
50. Kobryn,K., Lavoie,B.D. and Chaconas,G. (1999) Supercoiling-dependent site-specific binding of HU to naked Mu DNA. *J. Mol. Biol.*, **289**, 777–784.
51. Lal,A., Dhar,A., Trostel,A., Kouzine,F., Seshasayee,A.S.N. and Adhya,S. (2016) Genome scale patterns of supercoiling in a bacterial chromosome. *Nat. Commun.*, **7**, 11055.
52. Strick,T.R., Allemand,J.-F., Bensimon,D., Bensimon,A. and Croquette,V. (1996) The elasticity of a single supercoiled DNA molecule. *Science*, **271**, 1835–1837.
53. Cluzel,P., Lebrun,A., Heller,C., Lavery,R., Viovy,J.-L., Chatenay,D. and Caron,F. (1996) DNA: an extensible molecule. *Science*, **271**, 792–794.
54. Smith,S.B., Cui,Y. and Bustamante,C. (1996) Overstretching B-DNA: the elastic response of individual double-stranded and single-stranded DNA molecules. *Science*, **271**, 795–798.
55. Wang,M.D., Yin,H., Landick,R., Gelles,J. and Block,S.M. (1997) Stretching DNA with optical tweezers. *Biophys. J.*, **72**, 1335–1346.
56. Bryant,Z., Stone,M.D., Gore,J., Smith,S.B., Cozzarelli,N.R. and Bustamante,C. (2003) Structural transitions and elasticity from torque measurements on DNA. *Nature*, **424**, 338–341.
57. Yan,J., Skoko,D. and Marko,J.F. (2004) Near-field-magnetic-tweezer manipulation of single DNA molecules. *Phys. Rev. E*, **70**, 011905.

58. Deufel,C., Forth,S., Simmons,C.R., Dejgosha,S. and Wang,M.D. (2007) Nanofabricated quartz cylinders for angular trapping: DNA supercoiling torque detection. *Nat. Methods*, **4**, 223–225.
59. Lipfert,J., Kerssemakers,J.W.J., Jager,T. and Dekker,N.H. (2010) Magnetic torque tweezers: measuring torsional stiffness in DNA and RecA-DNA filaments. *Nat. Methods*, **7**, 977–980.
60. Janssen,X.J. A., Lipfert,J., Jager,T., Daudey,R., Beekman,J. and Dekker,N.H. (2012) Electromagnetic torque tweezers: a versatile approach for measurement of single-molecule twist and torque. *Nano Lett.*, **12**, 3634–3639.
61. Forth,S., Sheinin,M.Y., Inman,J. and Wang,M.D. (2013) Torque measurement at the single-molecule level. *Annu. Rev. Biophys.*, **42**, 583–604.
62. Katritch,V., Bustamante,C. and Olson,W.K. (2000) Pulling chromatin fibers: computer simulations of direct physical micromanipulations. *J. Mol. Biol.*, **295**, 29–40.
63. Aumann,F., Lankas,F., Caudron,M. and Langowski,J. (2006) Monte Carlo simulation of chromatin stretching. *Phys. Rev. E*, **73**, 041927.
64. Zhang,H. and Marko,J.F. (2010) Intrinsic and force-generated cooperativity in a theory of DNA-bending proteins. *Phys. Rev. E*, **82**, 051906.
65. Kepper,N., Ettig,R., Stehr,R., Marnach,S., Wedemann,G. and Rippe,K. (2011) Force spectroscopy of chromatin fibers: extracting energetics and structural information from Monte Carlo simulations. *Biopolymers*, **95**, 435–447.
66. Ettig,R., Kepper,N., Stehr,R., Wedemann,G. and Rippe,K. (2011) Dissecting DNA-histone interactions in the nucleosome by molecular dynamics simulations of DNA unwrapping. *Biophys. J.*, **101**, 1999–2008.
67. Collepardo-Guevara,R. and Schlick,T. (2011) The effect of linker histone's nucleosome binding affinity on chromatin unfolding mechanisms. *Biophys. J.*, **101**, 1670–1680.
68. Collepardo-Guevara,R. and Schlick,T. (2012) Crucial role of dynamic linker histone binding and divalent ions for DNA accessibility and gene regulation revealed by mesoscale modeling of oligonucleosomes. *Nucleic Acids Res.*, **40**, 8803–8817.
69. Zhang,H. and Marko,J.F. (2012) Range of interaction between DNA-bending proteins is controlled by the second-longest correlation length for bending fluctuations. *Phys. Rev. Lett.*, **109**, 248301.
70. Dobrovolskaia,I.V. and Arya,G. (2012) Dynamics of forced nucleosome unraveling and role of nonuniform histone-DNA interactions. *Biophys. J.*, **103**, 989–998.
71. Nam,G.-M. and Arya,G. (2014) Torsional behavior of chromatin is modulated by rotational phasing of nucleosomes. *Nucleic Acids Res.*, **42**, 9691–9699.
72. Elbel,T. and Langowski,J. (2015) The effect of DNA supercoiling on nucleosome structure and stability. *J. Phys. Condens. Matter*, **27**, 064105.
73. Dahlke,K. and Sing,C.E. (2018) Force-extension behavior of DNA in the presence of DNA-bending nucleoid associated proteins. *J. Chem. Phys.*, **148**, 084902.
74. Yan,J., Kawamura,R. and Marko,J.F. (2005) Statistics of loop formation along double helix DNAs. *Phys. Rev. E*, **71**, 061905.
75. Efremov,A.K., Winardhi,R.S. and Yan,J. (2016) Transfer-matrix calculations of DNA polymer micromechanics under tension and torque constraints. *Phys. Rev. E*, **94**, 032404.
76. Efremov,A.K., Winardhi,R.S. and Yan,J. (2017) Theoretical methods for studying DNA structural transitions under applied mechanical constraints. *Polymers*, **9**, 74.
77. Allemand,J.F., Bensimon,D., Lavery,R. and Croquette,V. (1998) Stretched and overwound DNA forms a Pauling-like structure with exposed bases. *Proc. Natl. Acad. Sci. U.S.A.*, **95**, 14152–14157.
78. Léger,J.F., Romano,G., Sarkar,A., Robert,J., Bourdieu,L., Chatenay,D. and Marko,J.F. (1999) Structural transitions of a twisted and stretched DNA molecule. *Phys. Rev. Lett.*, **83**, 1066–1069.
79. Sheinin,M.Y. and Wang,M.D. (2009) Twist-stretch coupling and phase transition during DNA supercoiling. *Phys. Chem. Chem. Phys.*, **11**, 4800–4803.
80. Sheinin,M.Y., Forth,S., Marko,J.F. and Wang,M.D. (2011) Underwound DNA under tension: structure, elasticity, and sequence-dependent behaviors. *Phys. Rev. Lett.*, **107**, 108102.
81. Oberstrass,F.C., Fernandes,L.E. and Bryant,Z. (2012) Torque measurements reveal sequence-specific cooperative transitions in supercoiled DNA. *Proc. Natl. Acad. Sci. U.S.A.*, **109**, 6106–6111.
82. Marko,J.F. and Neukirch,S. (2013) Global force-torque phase diagram for the DNA double helix: structural transitions, triple points and collapsed plectonemes. *Phys. Rev. E*, **88**, 062722.
83. Gel'fand,I.M., Minlos,R.A. and Shapiro,Z.Ya. (1963) *Representations of the Rotation and Lorentz Groups and Their Applications*. Pergamon Press, NY.
84. Sarkar,A., Léger,J.-F., Chatenay,D. and Marko,J.F. (2001) Structural transitions in DNA driven by external force and torque. *Phys. Rev. E*, **63**, 051903.
85. Călugăreanu,G. (1961) Sur les classes d'isotopie des noeuds tridimensionels et leurs invariants. *Czech. Math. J.*, **11**, 588–625.
86. White,J.H. (1969) Self-linking and the Gauss integral in higher dimensions. *Am. J. Math.*, **91**, 693–728.
87. Fuller,F.B. (1978) Decomposition of the linking number of a closed ribbon: a problem from molecular biology. *Proc. Nati. Acad. Sci. U.S.A.*, **75**, 3557–3561.
88. Fain,B., Rudnick,J. and Östlund,S. (1997) Conformations of linear DNA. *Phys. Rev. E*, **55**, 7364–7368.
89. Bouchiat,C. and Mézard,M. (2000) Elastic rod model of a supercoiled DNA molecule. *Eur. Phys. J. E*, **2**, 377–402.
90. Moroz,J.D. and Nelson,P. (1998) Entropic elasticity of twist-storing polymers. *Macromolecules*, **31**, 6333–6347.
91. Bouchiat,C. and Mézard,M. (1998) Elasticity model of a supercoiled DNA molecule. *Phys. Rev. Lett.*, **80**, 1556–1559.
92. Kleinert,H. (2009) *Path Integrals in Quantum Mechanics, Statistics, Polymer Physics, and Financial Markets*. World Scientific Publishing, Singapore.
93. Forth,S., Deufel,C., Sheinin,M.Y., Daniels,B., Sethna,J.P. and Wang,M.D. (2008) Abrupt buckling transition observed during the plectoneme formation of individual DNA molecules. *Phys. Rev. Lett.*, **100**, 148301.
94. Lim,C.J., Whang,Y.R., Kenney,L.J. and Yan,J. (2012) Gene silencing H-NS paralogue StpA forms a rigid protein filament along DNA that blocks DNA accessibility. *Nucleic Acids Res.*, **40**, 3316–3328.
95. Winardhi,R.S., Fu,W., Castang,S., Li,Y., Dove,S.L. and Yan,J. (2012) Higher order oligomerization is required for H-NS family member MvaT to form gene-silencing nucleoprotein filament. *Nucleic Acids Res.*, **40**, 8942–8952.
96. Lim,C.J., Lee,S.Y., Teramoto,J., Ishihama,A. and Yan,J. (2013) The nucleoid-associated protein Dan organizes chromosomal DNA through rigid nucleoprotein filament formation in *E. coli* during anoxia. *Nucleic Acids Res.*, **41**, 746–753.
97. Qu,Y., Lim,C.J., Whang,Y.R., Liu,J. and Yan,J. (2013) Mechanism of DNA organization by Mycobacterium tuberculosis protein Lsr2. *Nucleic Acids Res.*, **41**, 5263–5272.
98. Winardhi,R.S., Gulvady,R., Mellies,J.L. and Yan,J. (2014) Locus of enterocyte effacement-encoded regulator (Ler) of pathogenic *Escherichia coli* competes off histone-like nucleoid-structuring protein (H-NS) through noncooperative DNA binding. *J. Biol. Chem.*, **289**, 13739–13750.
99. Hamiche,A., Carot,V., Alilat,M., De Lucia,F., O'Donohue,M.-F., Révet,B. and Prunell,A. (1996) Interaction of the histone $(H3\text{-}H4)_2$ tetramer of the nucleosome with positively supercoiled DNA minicircles: potential flipping of the protein from a left- to a right-handed superhelical form. *Proc. Natl. Acad. Sci. U.S.A.*, **93**, 7588–7593.
100. Vlijm,R., Lee,M., Lipfert,J., Lusser,A., Dekker,C. and Dekker,N.H. (2015) Nucleosome assembly dynamics involve spontaneous fluctuations in the handedness of tetrasomes. *Cell Rep.*, **10**, 216–225.
101. Dong,F. and van Holde,K.E. (1991) Nucleosome positioning is determined by the $(H3\text{-}H4)_2$ tetramer. *Proc. Natl. Acad. Sci. U.S.A.*, **88**, 10596–10600.
102. Yan,J., Maresca,T.J., Skoko,D., Adams,C.D., Xiao,B., Christensen,M.O., Heald,R. and Marko,J.F. (2007) Micromanipulation studies of chromatin fibers in. *Xenopus* egg extracts reveal ATP-dependent chromatin assembly dynamics. *Mol. Biol. Cell*, **18**, 464–474.
103. Kruithof,M., Chien,F., de Jager,M. and van Noort,J. (2008) Subpiconewton dynamic force spectroscopy using magnetic tweezers. *Biophys. J.*, **94**, 2343–2348.

104. Prunell,A. (1998) A topological approach to nucleosome structure and dynamics: the linking number paradox and other issues. *Biophys. J.*, **74**, 2531–2544.
105. Lohr,D., Kovacic,R.T. and Van Holde,K.E. (1977) Quantitative analysis of the digestion of yeast chromatin by staphylococcal nuclease. *Biochemistry*, **16**, 463–471.
106. Shimamura,A., Tremethick,D. and Worcel,A. (1988) Characterization of the repressed 5S DNA minichromosomes assembled in vitro with a high-speed supernatant of *Xenopus laevis* oocytes. *Mol. Cell. Biol.*, **8**, 4257–4269.
107. Lagarias,J.C., Reeds,J.A., Wright,M.H. and Wright,P.E. (1998) Convergence properties of the Nelder–Mead simplex method in low dimensions. *SIAM J. Optim.*, **9**, 112–147.
108. Bustamante,C., Marko,J.F., Siggia,E.D. and Smith,S. (1994) Entropic elasticity of lambda-phage DNA. *Science*, **265**, 1599–1600.
109. Mosconi,F., Allemand,J.F., Bensimon,D. and Croquette,V. (2009) Measurement of the torque on a single stretched and twisted DNA using magnetic tweezers. *Phys. Rev. Lett.*, **102**, 078301.
110. Wang,J.C. (1979) Helical repeat of DNA in solution. *Proc. Natl. Acad. Sci. U.S.A.*, **76**, 200–203.